MetOcean Solutions

NUMERCIAL MODELLING OF THE WAIKOUAITI ESTUARY

Characterisation of the hydrodynamics and investigation of the influence of summer low flows on the physical and chemical condition of the estuary.

Report prepared for
Otago Regional Council

Specialists in Oceanography and Meteorology

MetOcean Solutions Ltd: Report Number P0287-01

August 2016

Report Status

Version	Date	Status	Approved by
RevA	26/07/2016	Draft for internal review	Zynfogel
RevB	08/08/2016	Draft for client review	McComb
RevC	24/08/2016	Updated draft for client review	McComb
Rev0	31/08/2016	Approved for release	McComb

It is the responsibility of the reader to verify the currency of the version number of this report.

TABLE OF CONTENTS

LIST OF FIGURES

LIST OF TABLES

1. INTRODUCTION

The Otago Regional Council (ORC) requires an increased understanding of the hydrodynamics and the ecological condition of the Waikouaiti Estuary, specifically under low freshwater inflow scenarios during the summer months. To meet this need, a study program has been prescribed with three distinct stages:

Stage 1 Determination of estuary bathymetry.

Stage 2 Assessment of the influence of summer low flows on the physical and chemical condition of the estuary.

Stage 3 Assessment of the influence of changes in physical and chemical condition of the estuary as a result of low flows, on the ecology of the estuary.

The present report addresses Stages 1 and 2 of the study scope. The objective is to enable the progression of Stage 3 of the project and thereby assess the ecological influence arising from changes in physical and chemical conditions associated with the low flow scenarios for the estuary. Three flow states have been used to describe the low flow scenarios of the Waikouaiti River. The mean annual 7−day low flow (MALF) is 258 l/s and the default low flow scenario is 50% of this value (i.e. 129 l/s). The other required flows for testing are 220 l/s and 350 l/s.

The key deliverables for Stages 1 and 2 are:

- The presentation of a validated hydrodynamic model.
- Characterisation of the estuary in terms of the governing hydrodynamics.
- An assessment of the influence of estuary currents on sediment mobility and sediment transport capacity.
- An assessment of the influence of seawater on dilution in the estuary.
- An assessment of the influence of tidal volume on the wetted habitat.

This report is set out as follows. In Section 2 the data collection program is described, including summary plots of the main parameters. In Section 3 the numerical model is described, including information about the model domain, boundary conditions and the validation of the model against observation. In Section 4 the modelling results are presented, and a summary is given in Section 5.

2. ESTUARY MEASUREMENTS

A measurement program was established to provide the information necessary to establish the numerical model of the estuary, and provide data to validate the governing hydrodynamics. The measurement program was successfully completed over a 5-week period (12th March to 22nd April, 2016). The work was undertaken by staff from the Cawthron Institute (Figure 2.1).

Eleven instruments were deployed between the estuary mouth and Orbell's Crossing, some 4.5 km upstream. The suite of oceanographic instruments includes two FSI current meters, four RBR water level sensors, four Hobo temperature and salinity loggers. The measurement locations are shown in Figure 2.2, and the locations and further details are provided on Table 2.1. A full data recovery was made, with the exception of currents at the wharf, which suffered a sensor failure.

A bathymetry survey was undertaken by Hunter Hydrographics Ltd from the 8th to the 13th of March, 2016. The Survey Report is appended to this report.

Figure 2.1 Cawthron Institute staff and the *Kotare* used for instrument deployment and recovery operations.

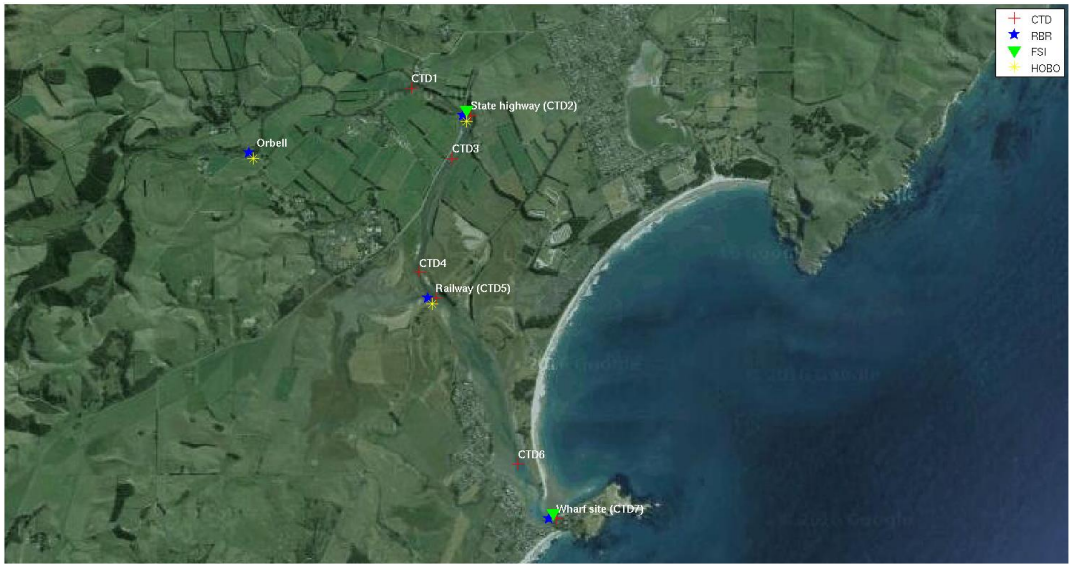

Figure 2.2 Aerial photo (Google Earth) of the Waikouaiti estuary showing the positions of all deployed instruments, this include 2 FSI (green triangles), 4 RBR (blue stars), 7 CTD deployments (red crosses) and 4 HOBO loggers (yellow stars).

Table 2.1 Duration, coordinates and approximate water depth the instruments deployed during the field campaigns.

Site	Instrument	Measurement parameters					Deployment duration		Coordinates		Water depth (MSL, m)
		Temp	Sal	Water level	Current	Chl, PAR, Turbidity, Do	start	end	Latitude	Longitude	
Orbell	RBR, HOBO	X	X	X			15/03/2016	21/04/2016	-45.6083	170.6238	1.0
CTD1	CTD	X	X			X	11/03/2016	11/03/2016	-45.6025	170.6436	1.0
State Highway (CTD2)	RBR, CTD, HOBO, FSI	X	X	X	X	X	11/03/2016	21/03/2016	-45.6049	170.6511	1.8
CTD3	CTD	X	X			X	11/03/2016	11/03/2016	-45.6088	170.6488	0.9
CTD4	CTD	X	X			X	11/03/2016	11/03/2016	-45.6190	170.6446	1.8
Railway (CTD5)	RBR, CTD, HOBO	X	X	X		X	11/03/2016	21/03/2016	-45.6213	170.6467	0.9
CTD6	CTD	X	X			X	11/03/2016	11/03/2016	-45.6362	170.6572	0.8
Wharf (CTD7)	RBR, CTD, FSI	X	X	X	X	X	11/03/2016	21/03/2016	-45.6410	170.6622	0.8

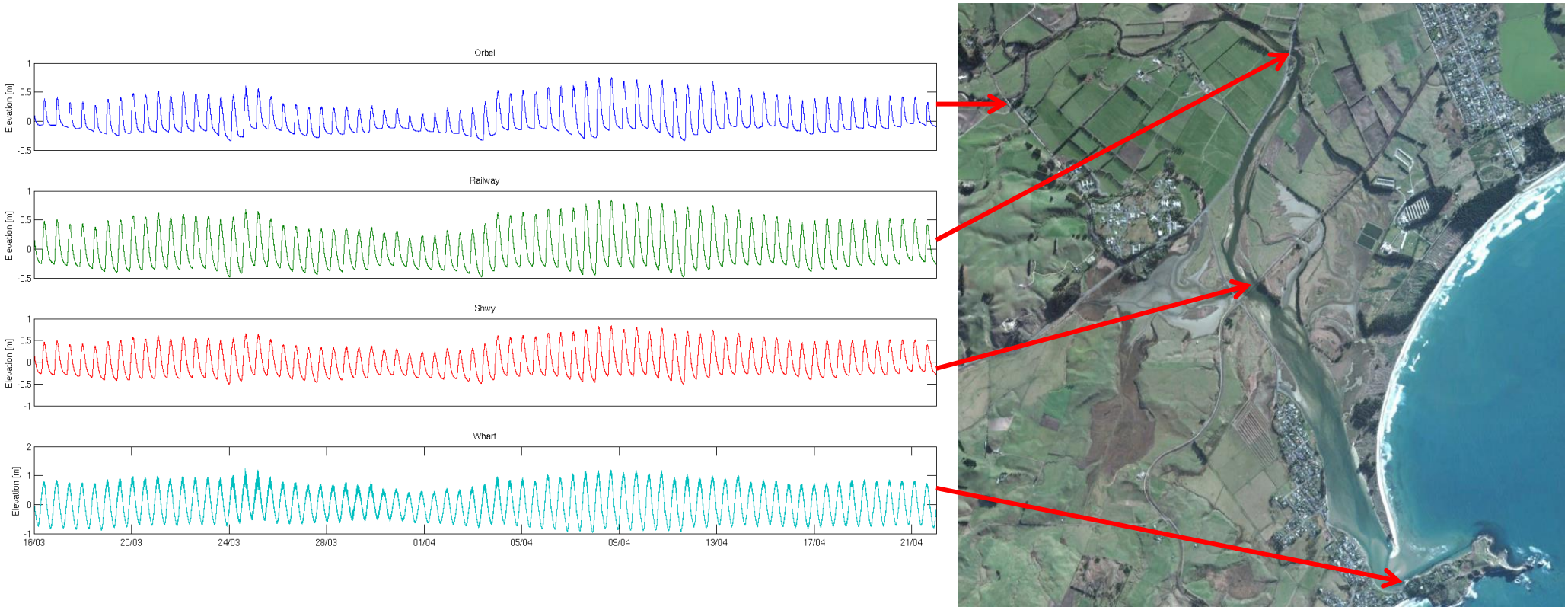

Figure 2.3 Water level measurement locations and time series data.

2.1. Water levels and currents

Water levels were measured with RBR pressure meters on fixed platforms at four locations. A complete record was collected, and the data are shown in Figure 2.3. Here, the pressure data have been converted to water levels with atmospheric correction.

Currents were measured in 5-minute bursts every 30 minutes, and the rose plot is shown on Figure 2.4. The highest measured velocity was 0.50 m/s, which occurred on an ebb flow when the measured river flow was around 250 l/s.

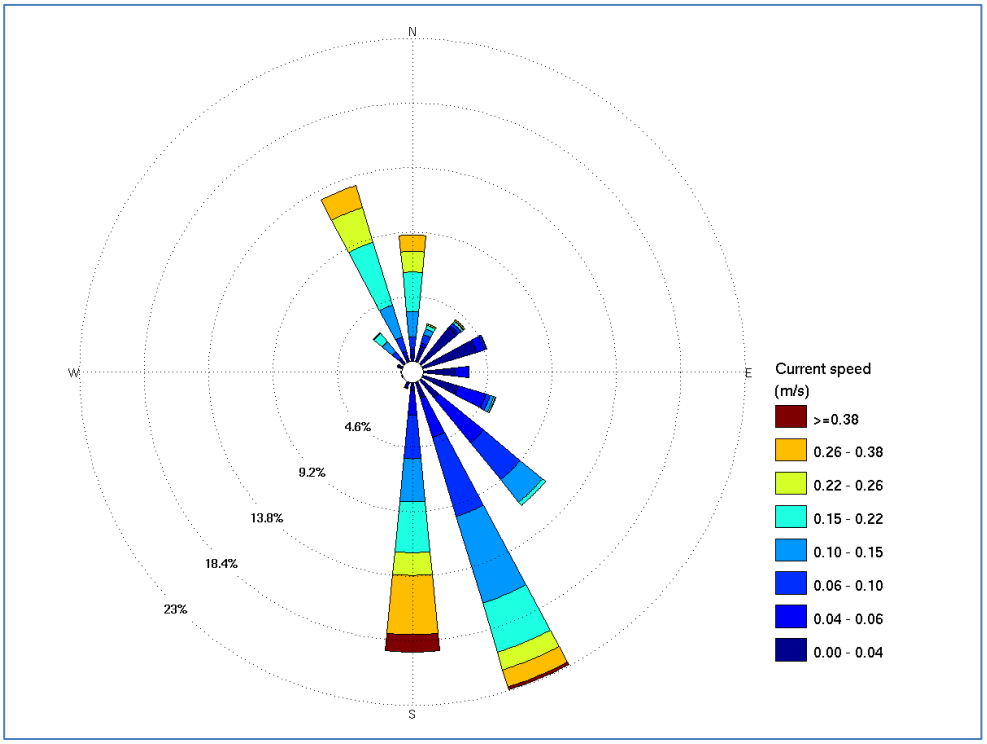

Figure 2.4 Measured current rose from adjacent to the State Highway Bridge.

2.2. Water column properties

Measurements of the water properties were undertaken at three fixed locations (seabed at Orbell and State Highway and surface and seabed at Railway, Table 2.1) using four Hobo conductivity and temperature sensors.

Profiling casts were made at each of the sites (except Orbell) on 11th March 2016. These casts recorded the temperature, conductivity, turbidity, fluorimeter, PAR (photosynthetically active radiation) and dissolved oxygen. Results are presented in Figure 2.5. Time series plots of nearbed temperature and salinity are presented in Figure 2.6 and Figure 2.7

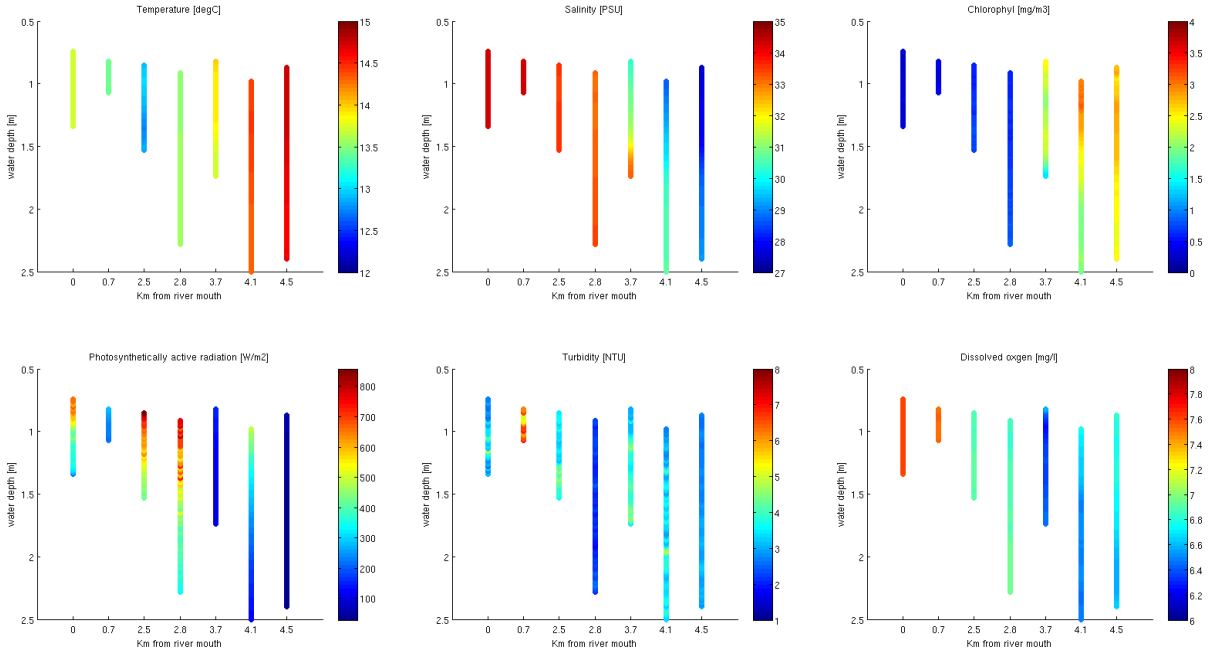

Figure 2.5 Profiling cast results collected at high tide on 11 March 2016, presented for six parameters with sequential distance from the estuary mouth.

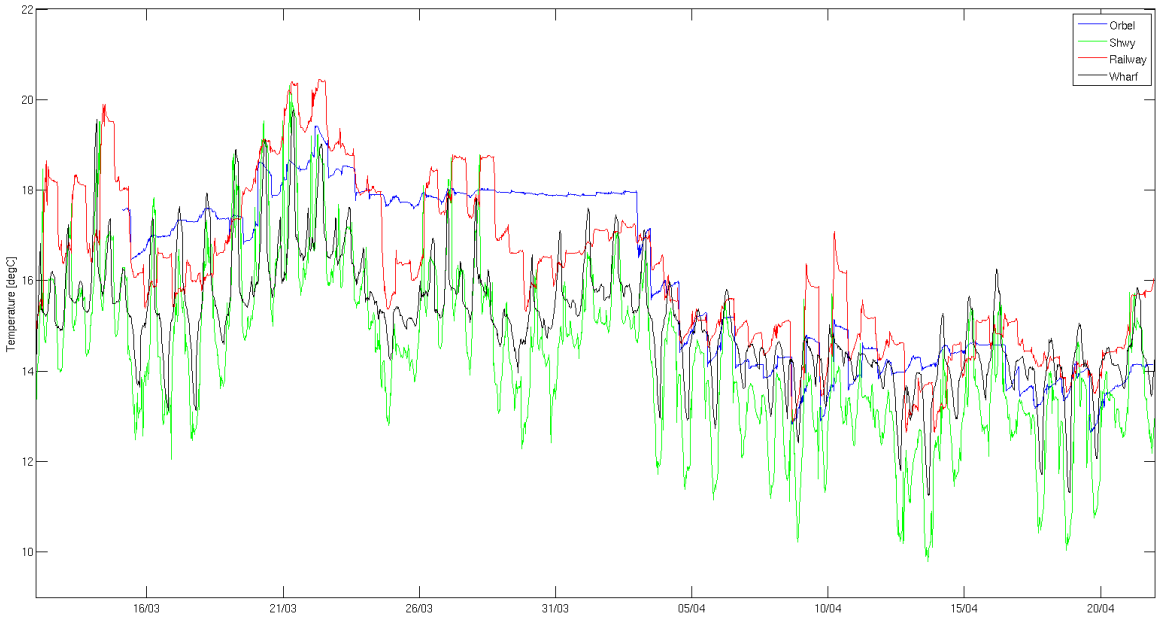

Figure 2.6 Time series plot showing the measured nearbed temperatures.

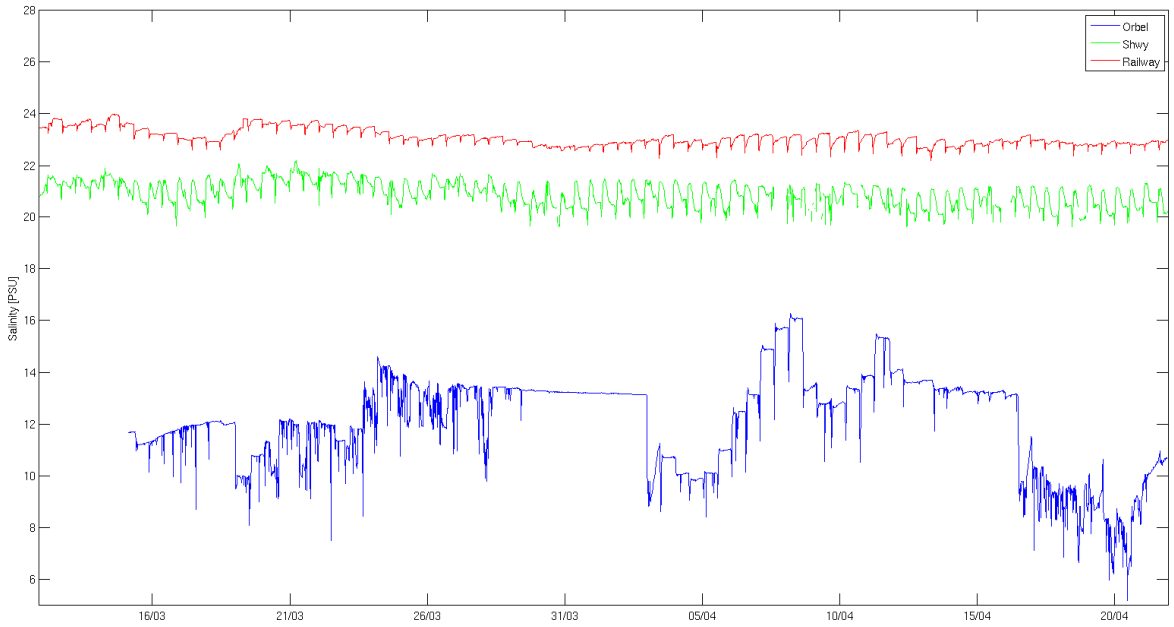

Figure 2.7 Time series plot showing the measured nearbed salinity.

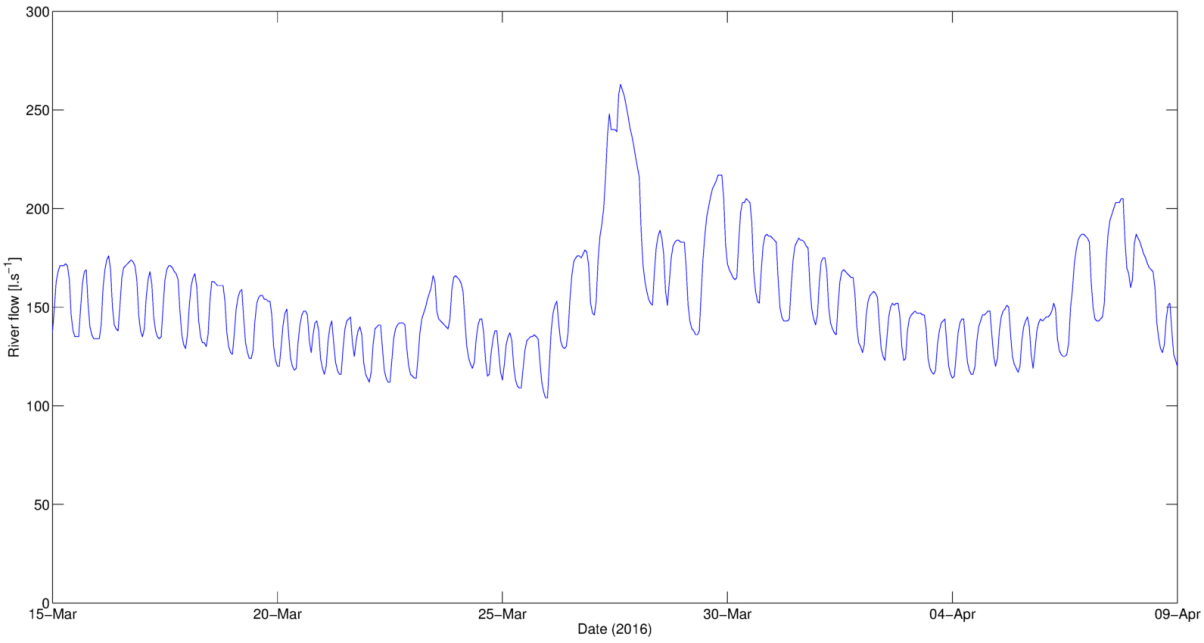

Figure 2.8 Time series plot showing the measured river flows from Orbell's Crossing.

3. THE HYDRODYNAMIC MODEL

3.1. Model description

The 3D modelling of the Waikouaiti Estuary has used the open-source model SCHISM[1],[2]. The benefit of using open-source science models is the full transparency of the code and the numerical schemes, and the ability for other researchers to replicate and enhance any previous modelling efforts for a given environment.

SCHISM is a prognostic finite-element unstructured-grid model designed to simulate 3D baroclinic, 3D barotropic or 2D barotropic circulation. The barotropic mode equations employ a semi-implicit finite-element Eulerian-Lagrangian algorithm to solve the shallow-water equations, forced by relevant physical processes (atmospheric, oceanic and fluvial forcing). A detailed description of the SCHISM model formulation, governing equations and numerics can be found in Zhang and Baptista (2008).

The finite-element grid structure (i.e. triangles) used by SCHISM has resolution and scale benefits over other regular or curvilinear based hydrodynamic models. SCHISM is computationally efficiently in the way resolves the shape and complex bathymetry associated with estuaries, while the governing equations are similar to other open source models such as Delft3D. SCHISM has been used extensively within the scientific community[3],[4] and forms the backbone to operational systems used to predict nowcast and forecast estuarine water levels, currents, water temperature and salinity[5].

3.2. Model domain

Four sources of data were combined to create the underlying bathymetric domain for the model (Figure 3.1). Primacy was given to the most recent survey data from March 2016, which was blended with the LIDAR from 2006 and interpreted with the latest aerial images.

The model resolution was optimised to ensure the salient hydrodynamic processes would be replicated. The offshore resolution is approximately 200 m, while inside the estuary the elements reduce to 5 m size. The triangular elements for the model are presented in Figure 3.2. The domain extends upstream beyond Orbell's Crossing and the full bathymetric domain is presented in Figure 3.3.

3.3. Boundary conditions

Offshore tidal elevation and velocity data are defined from a regional tide model that was previously validated for Port Otago. The offshore salinity and temperature regime was sourced from a hydrodynamic reanalysis of all New Zealand that used the ROMS model. River flow data from Orbell's Crossing was supplied by ORC.

[1] http://ccrm.vims.edu/schism/
[2] http://www.ccrm.vims.edu/w/index.php/Main_Page#SCHISM_WIKI
[3] http://www.stccmop.org/knowledge_transfer/software/selfe/publications
[4] http://ccrm.vims.edu/schism/schism_pubs.html
[5] https://tidesandcurrents.noaa.gov/ofs/creofs/creofs_info.html

3.4. Water age calculation with Eulerian tracers

Eulerian tracer is a field that obeys a classical advection-diffusion equation driven with currents of the hydrodynamic model (Meier and Höglund, 2013). Deleersnijder *et al.* (2001) presented a detailed description of Eulerian tracer theory applied to the age distribution of seawater. Sources, sinks and initial and boundary conditions are specified for the tracer under consideration. According to Zhang *et al.* (2010), the "mean tracer age" is calculated from the mean of the spectrum, which is defined as "the mass-weighted, arithmetic average of the time elapsed since the tracer left the source region". The "mean residence time" is defined as "the mass-weighted, arithmetic average of the time needed for the tracer to leave a domain of interest". The water age represents the mean age of the water in a grid cell of the numerical model used, and this value results from the mixing of water parcels of different ages within each cell (Andrejev et al., 2004). A detailed description of Eulerian tracer technique to obtain water age and residence time is presented in Zhang *et al.* (2010). These authors investigated the time scales associated with the spreading of the Hudson River source waters across the inner shelf of New York Bight. Differing from the common Lagrangian approach, which is characterised by the release of many tracers and extracting time-scale information from their differential transport, Eulerian tracer technique is computationally much cheaper (Zhang et al., 2010). However, it does not give full details with regards to the water parcel composition and age, as it gives average age inside each grid cell. Still it is a very useful technique for studying spatial patterns of circulation and mixing and the associated time scales (Hall and Haine, 2002; Zhang et al., 2010).

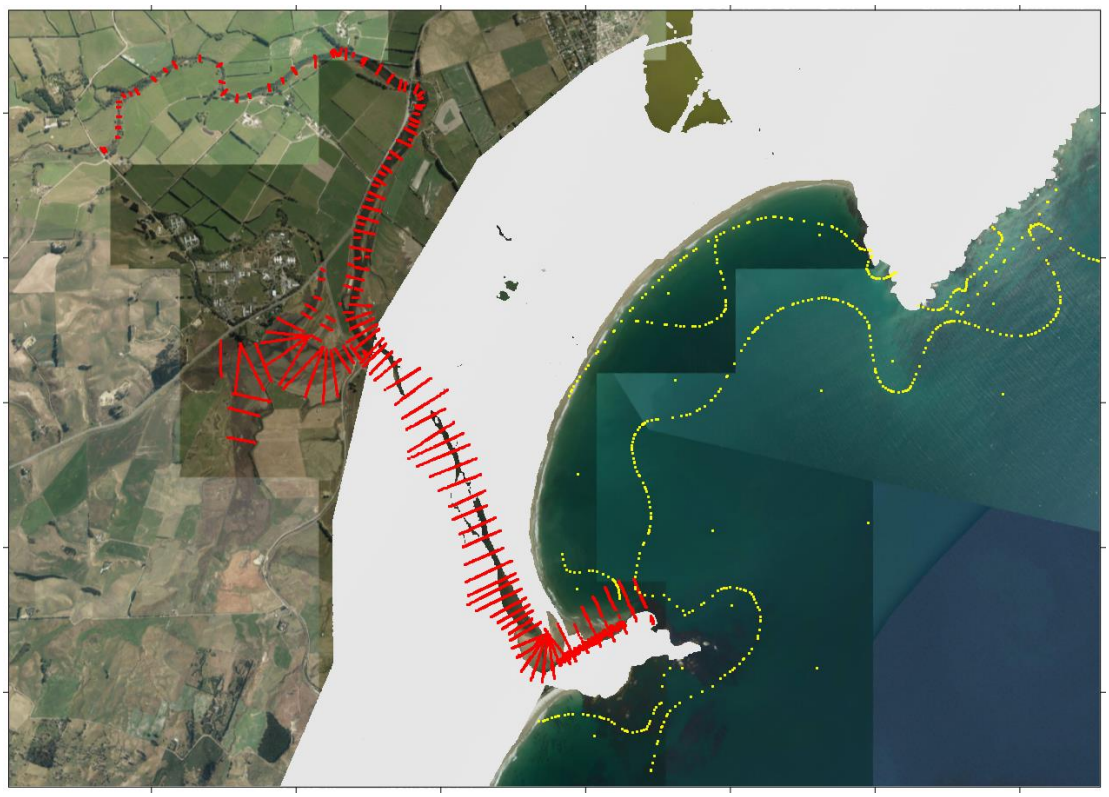

Figure 3.1 Bathymetry sources used to prepare the model domain. White is from the 2006 LIDAR survey, yellow is the LINZ navigational chart contours, and red is the March 2016 hydrographic survey lines.

Figure 3.2 Triangular model mesh defined for the Waikouaiti Estuary. Right is the extent of the domain, and left is a zoom on the central part of the estuary.

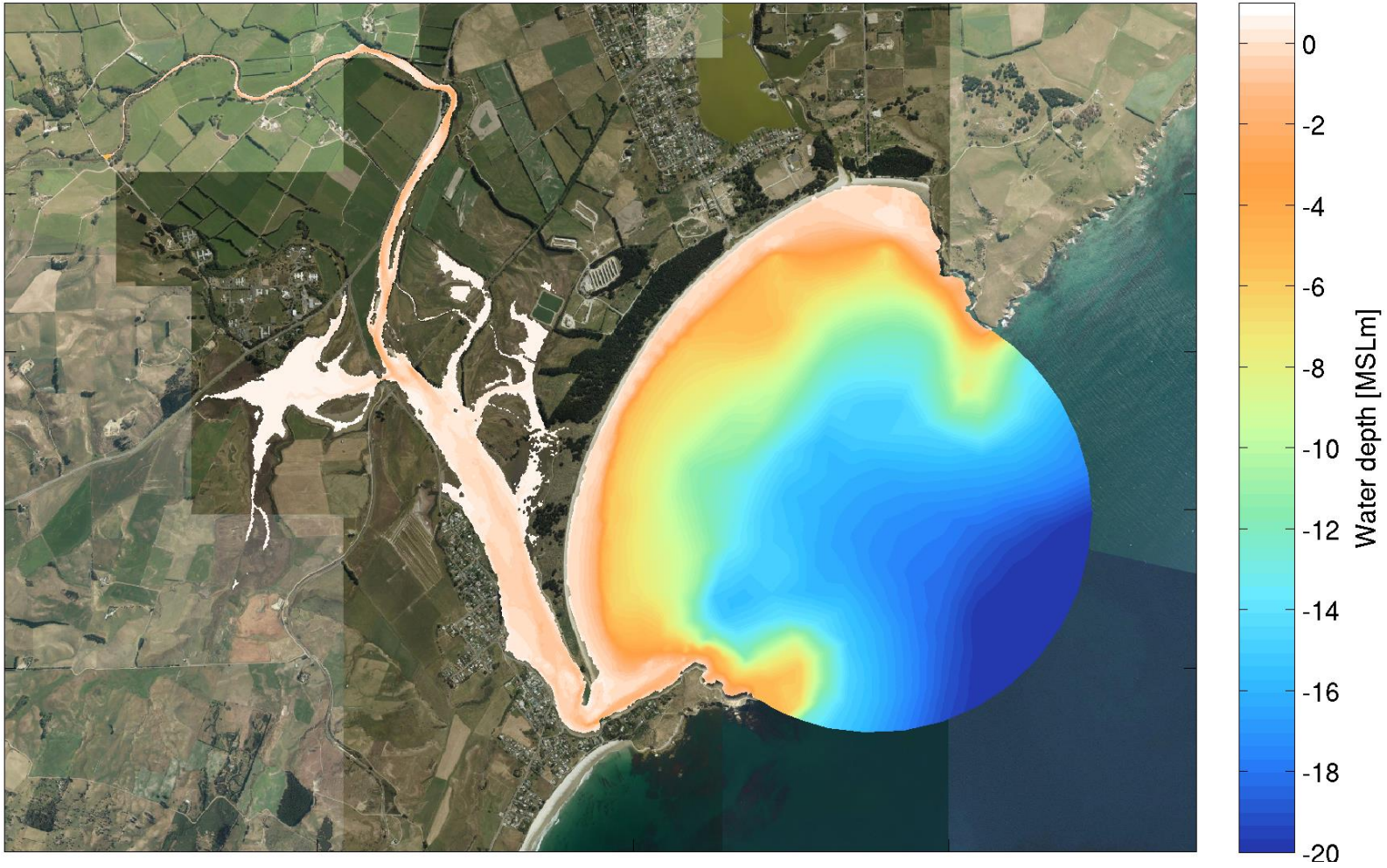

Figure 3.3 SCHISM bathymetric domain for the Waikouaiti Estuary.

3.5. Validation of the model hydrodynamics

The ability of the model to replicate the tidal dynamics of the estuary was made by directly comparing the measured water levels at four locations and the current speed and direction from near the State Highway Bridge with the predictions from the model at the same location. Note the model was forced with tidal and fluvial boundaries.

The validation for water level shows the model is effectively replicating the tidal boundary conditions near the entrance, and also the magnitude and asymmetry of the tidal curve throughout the length of the estuary. A time series plot showing the measured and modelled wave levels over a one-week period is presented in Figure 3.4. The validation for current speed (Figure 3.5) indicates the model provides a very creditable representation of the complex flow regime, with the phase and magnitude of the ebb and flood tidal stages being captured. Combined, the validation of water level and flow indicates the model can adequately reproduce the primary tidal hydrodynamics of the estuary.

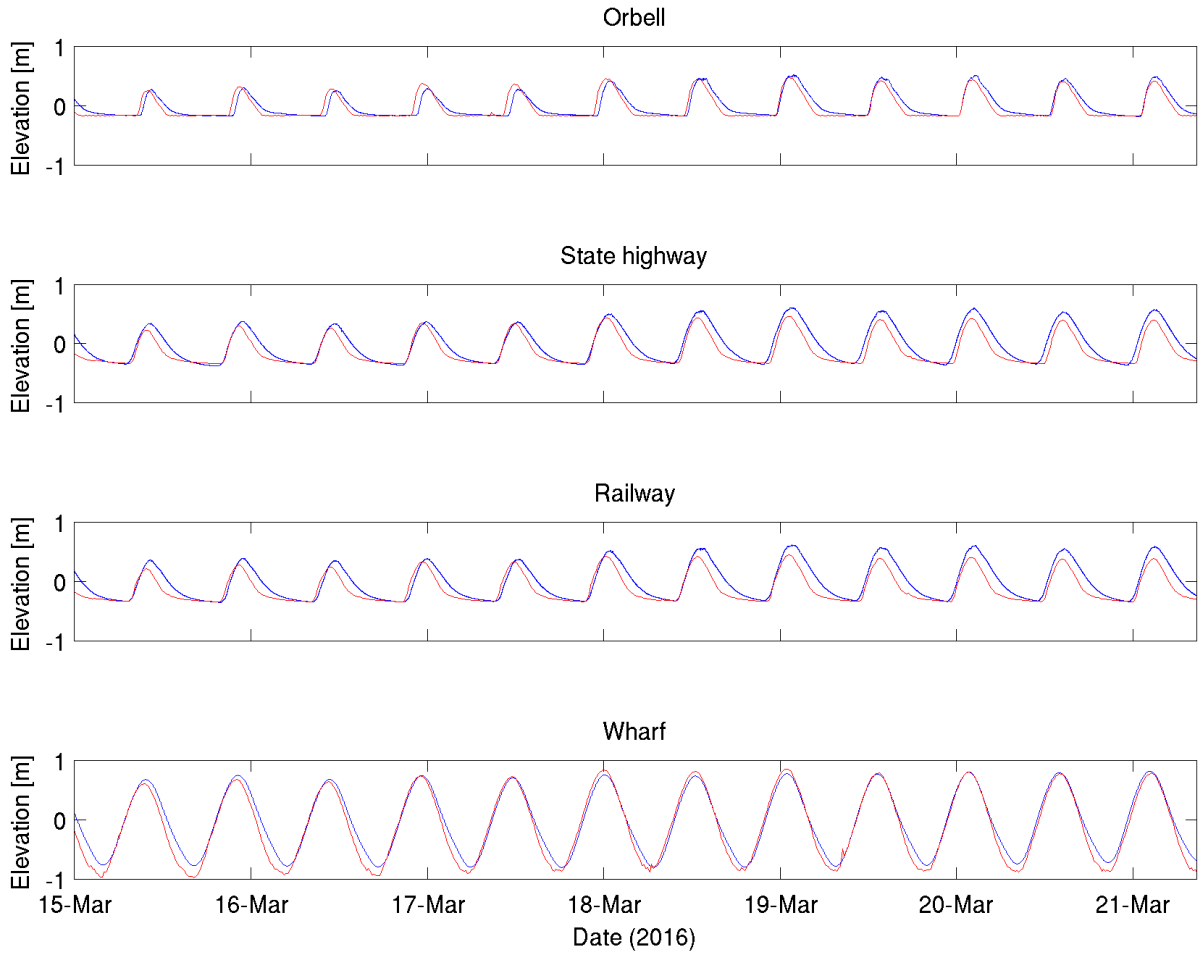

Figure 3.4 Numerical model validation against water levels measured at four sites. The measured data is shown in blue and the model predictions are in red.

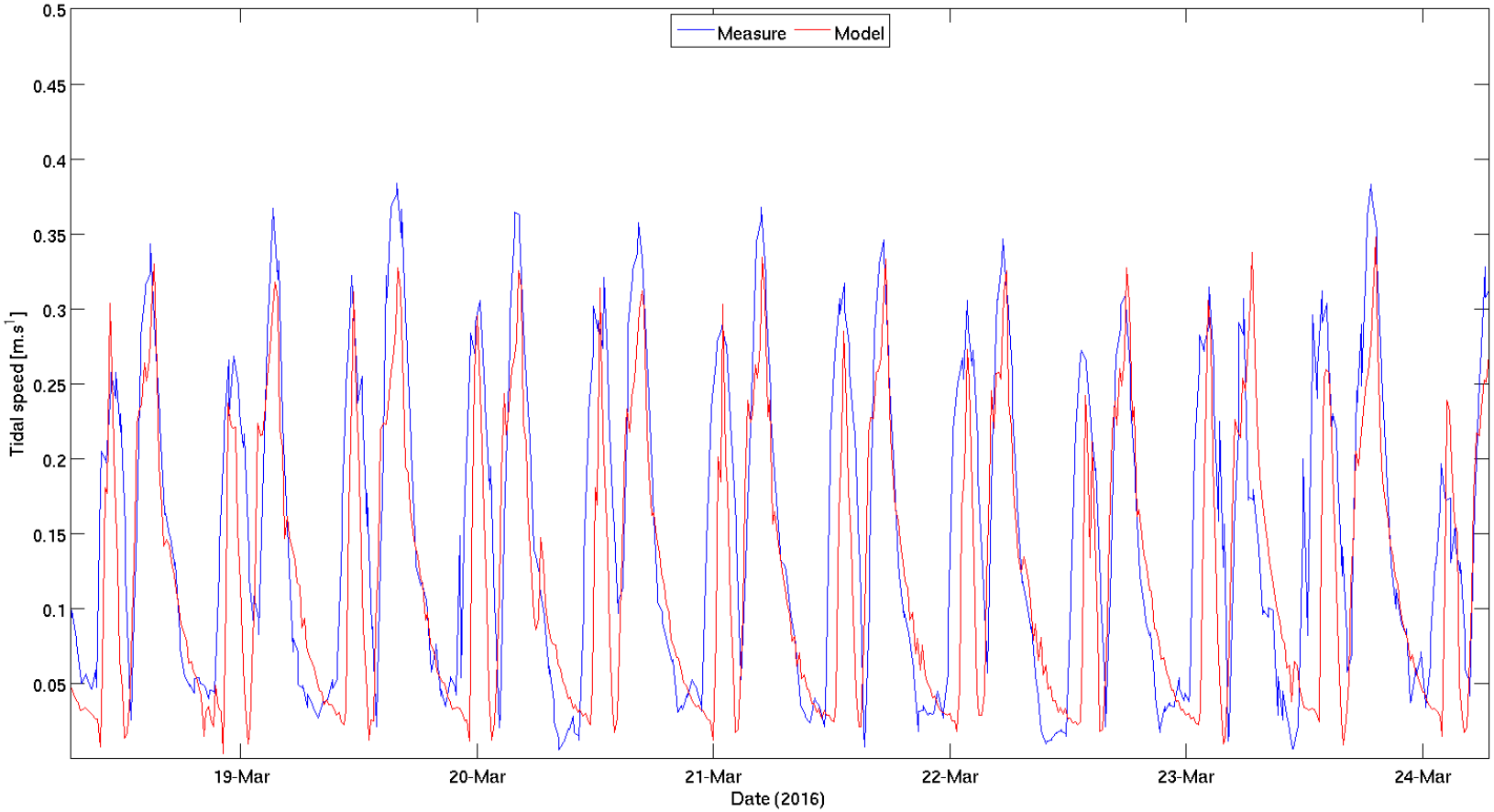

Figure 3.5 Model validation against the current speed measured near the State Highway bridge. The measured data is shown in blue and the model predictions are in red.

4. MODEL RESULTS

4.1. Governing dynamics

The model has been used to characterise the estuary in terms of the governing hydrodynamics.

Firstly, the peak tidal flow regime under spring and neap conditions for ebb and flood states was modelled with a reference river flow rate of 350 l/s. These results, presented in Figure 4.1 and Figure 4.2; showing clear differences in the depth-averaged flow between the ebb and flood stages. For example, near the entrance the ebb tide is a well-defined jet while the flood is represented by a more diffuse movement of water into the estuary. The flow regime is illustrated in time series at three arbitrary locations on Figure 4.3. Here, the asymmetry in the tidal flow is clearly evident and how it varied through the estuary. For example, the flood tide flow is stronger than the ebb tide flow at the lower and upper sites in Figure 4.3, but opposite is true for the mid-estuary location, which is a consequence of the greater cross-sectional area of the estuary immediately downstream of the Railway bridge.

The model has been used to make an initial assessment of the sediment mobility and transport capacity within the estuary. Currents impart a stress on the estuary sediments, and when that stress exceeds an entrainment threshold, the sediments can be mobilised and transported by the flows. Maps showing the shear stress at the peak flow on spring tides during the ebb and flood tide have been produced, and these are presented in Figure 4.4. As with the peak current speeds, there are clear differences in the peak shear stress for the ebb and flood stages. For example during the flood stage the peak stress has a broad influence over the entrance region and extends further into the estuary than the ebb state, which exhibits a highly constrained pattern. The spatial distribution of peak shear stress has a defining role on the composition of the bed sediments in the estuary as well as the benthic communities that inhabit them. Coarse material requires higher current flows to mobilise than fine material, and the duration of the flow above this critical entrainment level is also very important to the sediment transport outcomes. The model shows a very different pattern between and the ebb and the flood tide stages and over the spring-neap cycles the duration and magnitude exhibits variation as well.

The net consequence of the strong tidal asymmetry in mobilising and entraining the bed sediments leads to sorting of the grain sizes over time. While equilibrium develops, it is unsurprising that changes to estuary morphology occur when one of the forces or fluxes is altered, even quite subtly. For example, an energetic north-easterly storm sea that occurs over the flood tide may result in sand influx to the estuary that takes several months to flush out. Or, accretion of fine material on the flanks of the central estuary following heavy rainfall may lead to deepening of the main channels as a result of the increased shear stress. Ultimately, the system is complex and it exists in a fine balance; the benefit of a model is that aspects of the dynamics, such as the asymmetry, can be examined and the effects of changes can be estimated.

Tests with the lower river flow rates (i.e. 129 and 220 l/s) showed that the bed shear stresses are dominated by tidal currents, and the effect of river flows up to 350 l/s on the main body of the estuary is negligible.

Of further interest is the percentage of time during the spring and neap tides that the bed has the potential to be mobilised. In Figure 4.5 and Figure 4.6 the percentage time exceedance has been calculated for three representative grain sizes, ranging from silt to fine sand (i.e. 50, 100 and 200 microns). A 350 l/s river flow regime was included in these calculations. Sedimentation is influenced by supply and flux, so the zones with high entrainment and transport potential (e.g. near the entrance) require adequate sediment supply in order to maintain equilibrium, else a coarsening of the bed sediments will occur. Notably, even the smaller channels have flows that entrain silts and sands for considerable periods of time on each tide, whereas the adjacent flats do not, and these areas are more susceptible to siltation.

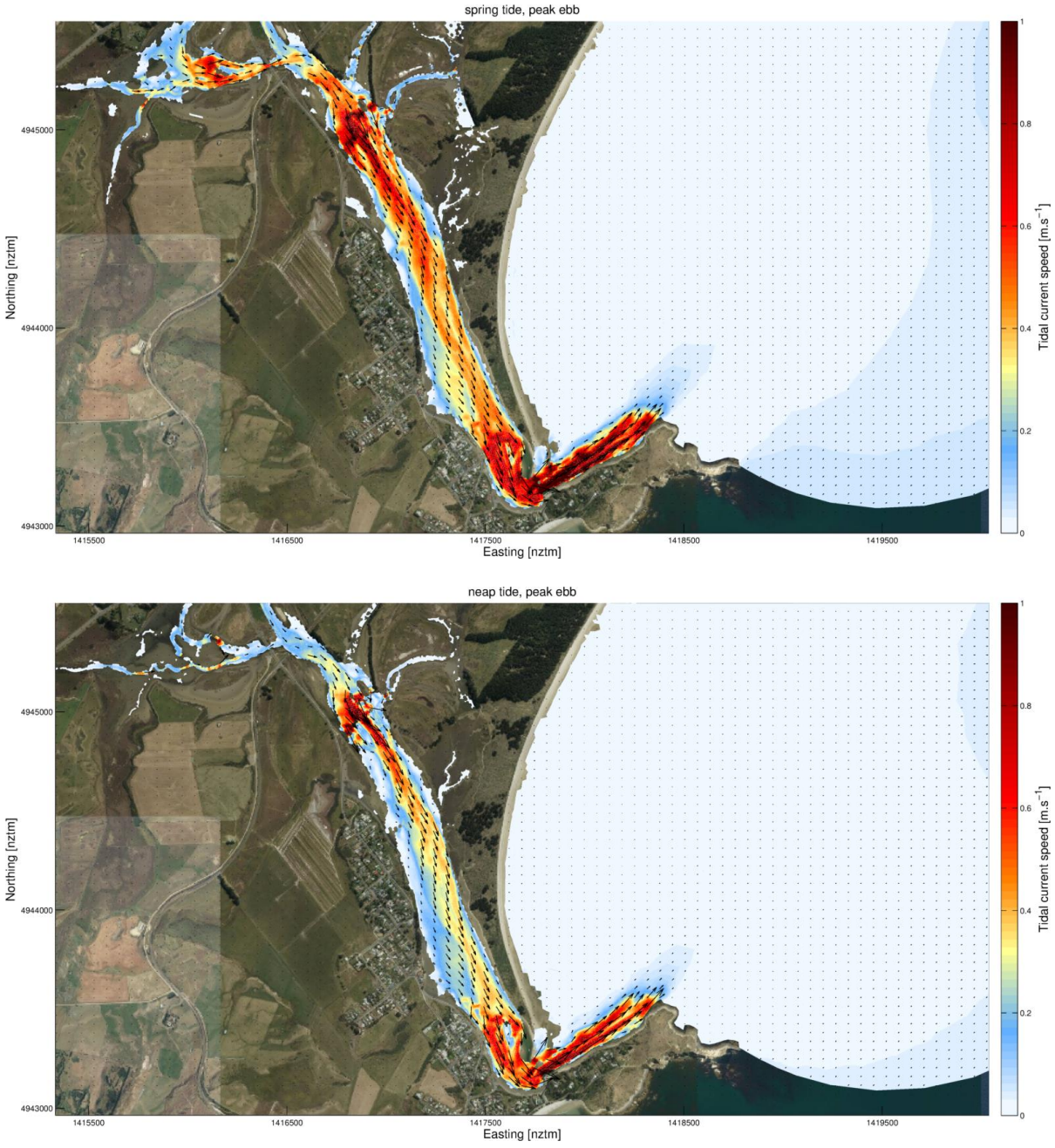

Figure 4.1 Snapshot of peak ebb tidal velocity at the estuary entrance during spring (top) and neap (bottom) tide.

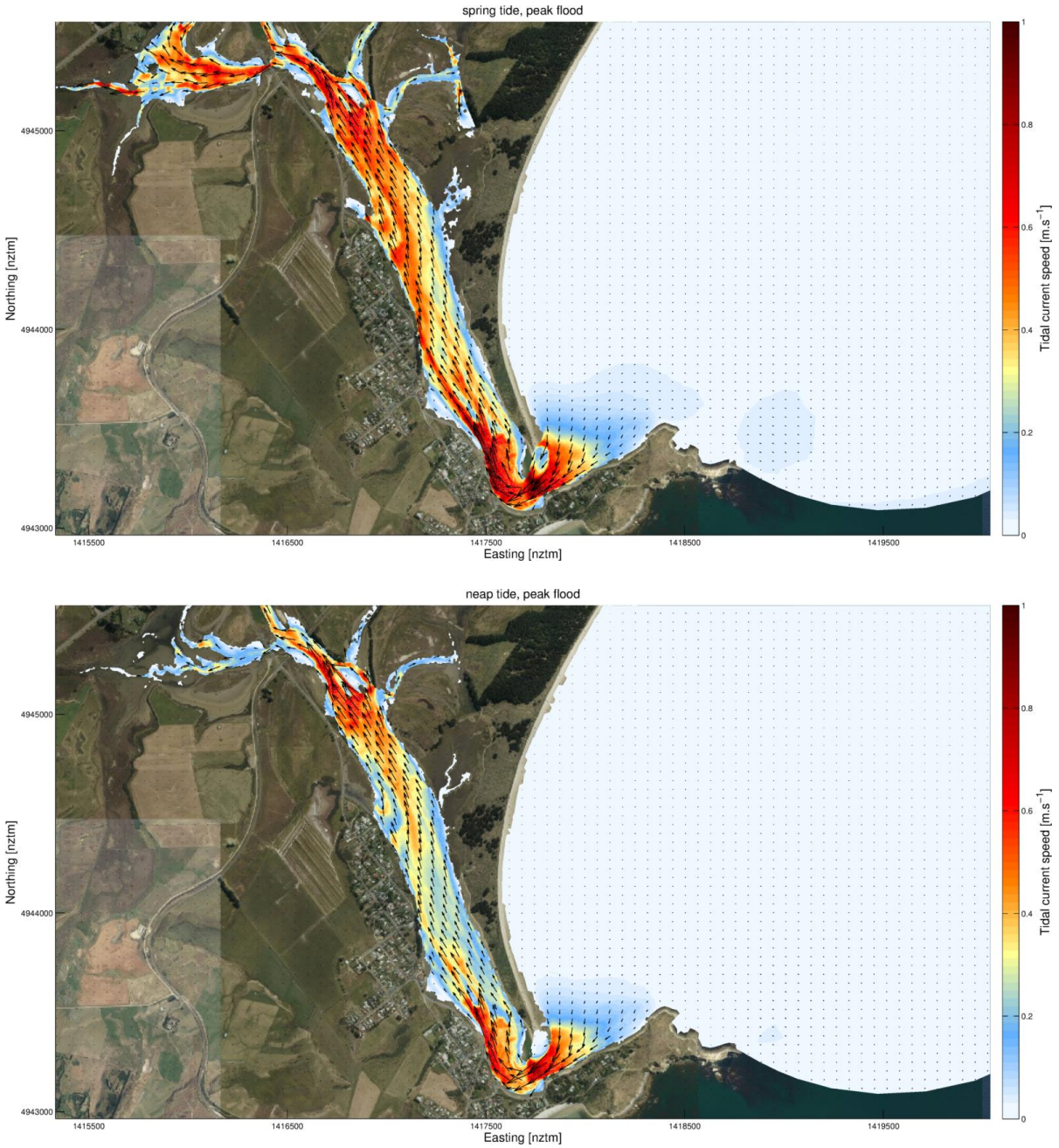

Figure 4.2 Snapshot of peak flood tidal velocity at the estuary entrance during spring (top) and neap (bottom) tide.

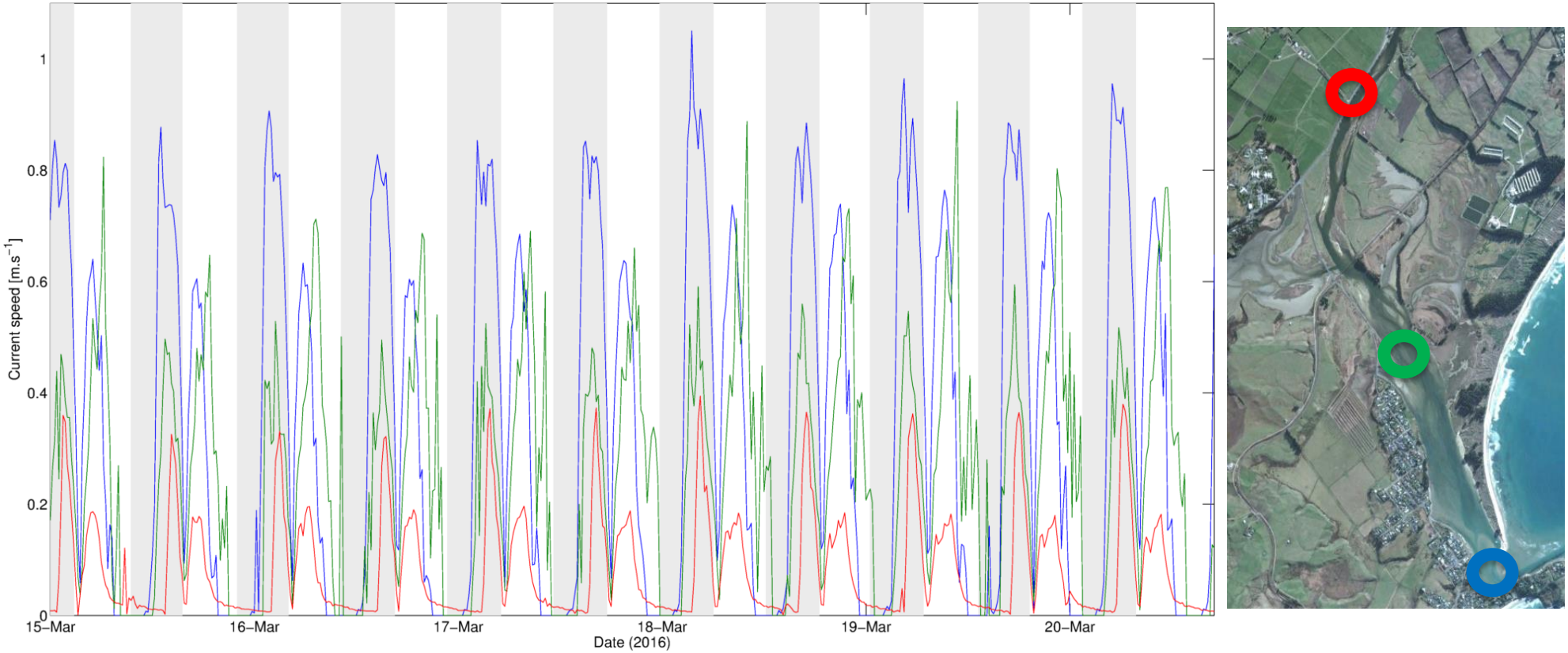

Figure 4.3 Example time series of tidal currents predicted by the model at three locations in the estuary (blue = lower section, green = middle section and red = upper section), as indicated on the aerial photo. The light shading identifies the time between low water and high water.

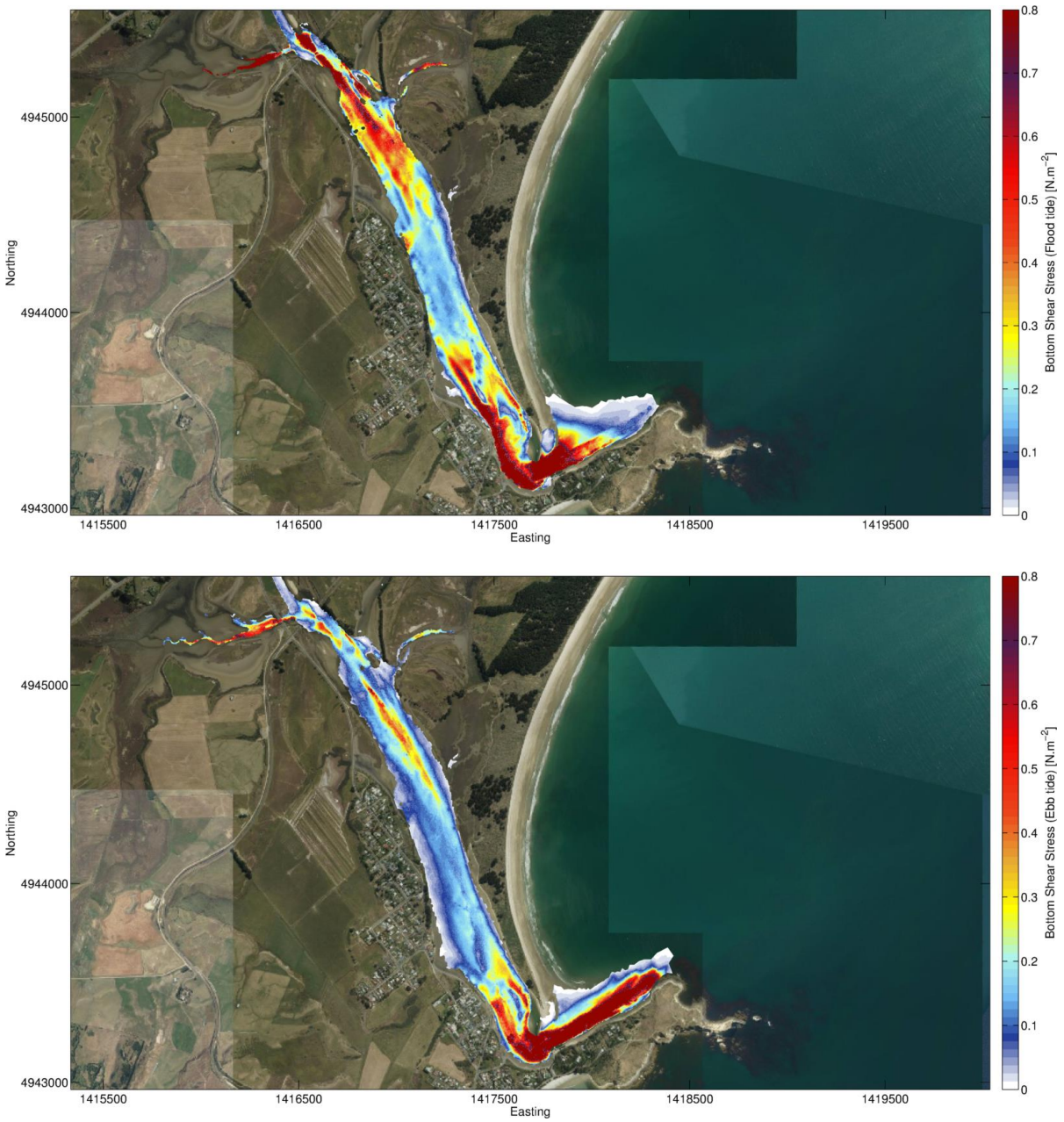

Figure 4.4 Bottom shear stress in spring tide during peak flood (top) and peak ebb (bottom).

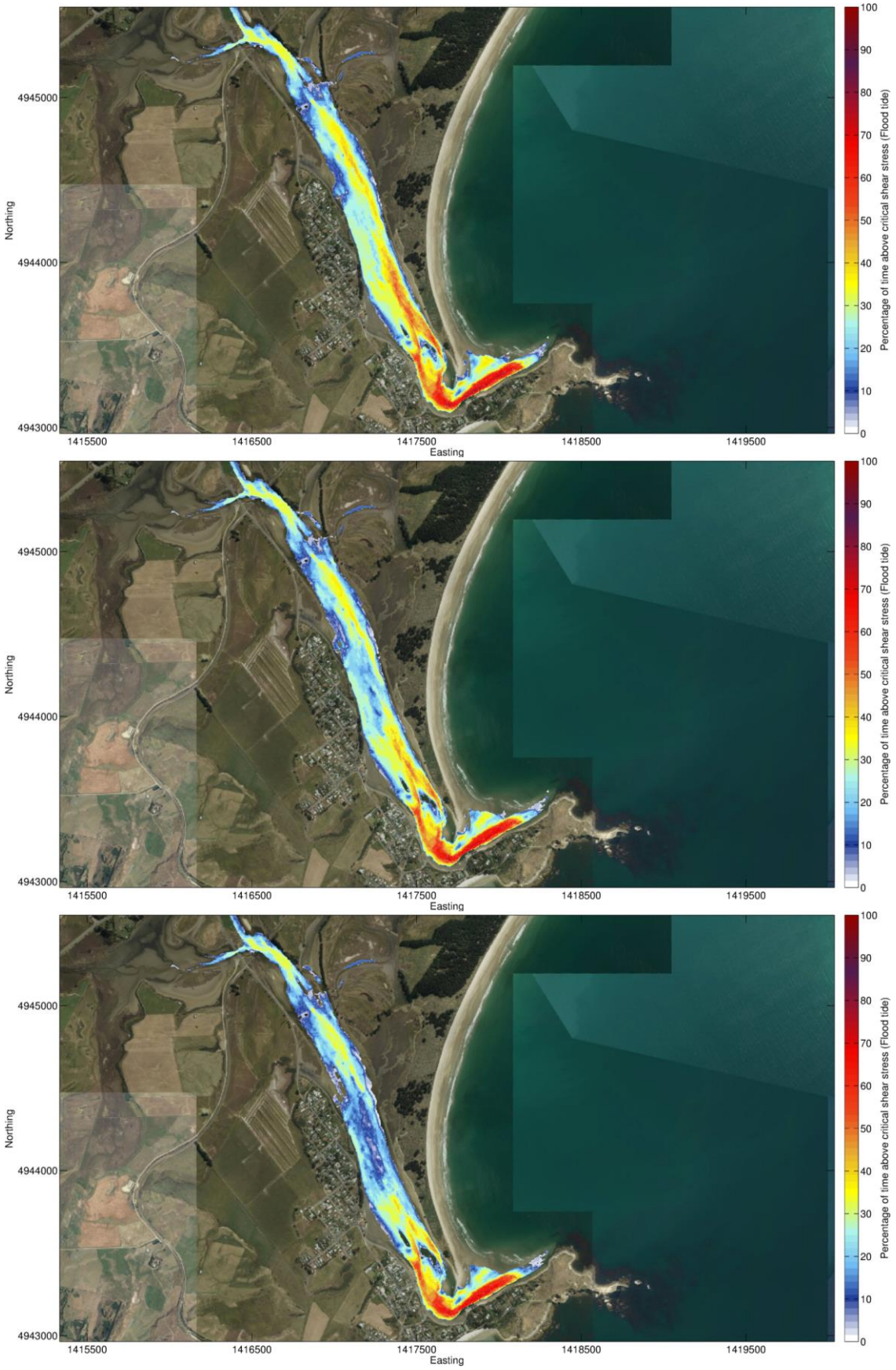

Figure 4.5 Percentage of time the critical bed shear stress is exceeded in spring tide during flood for D50 grain size value of 50 (top), 100 (middle) and 200 (bottom) microns.

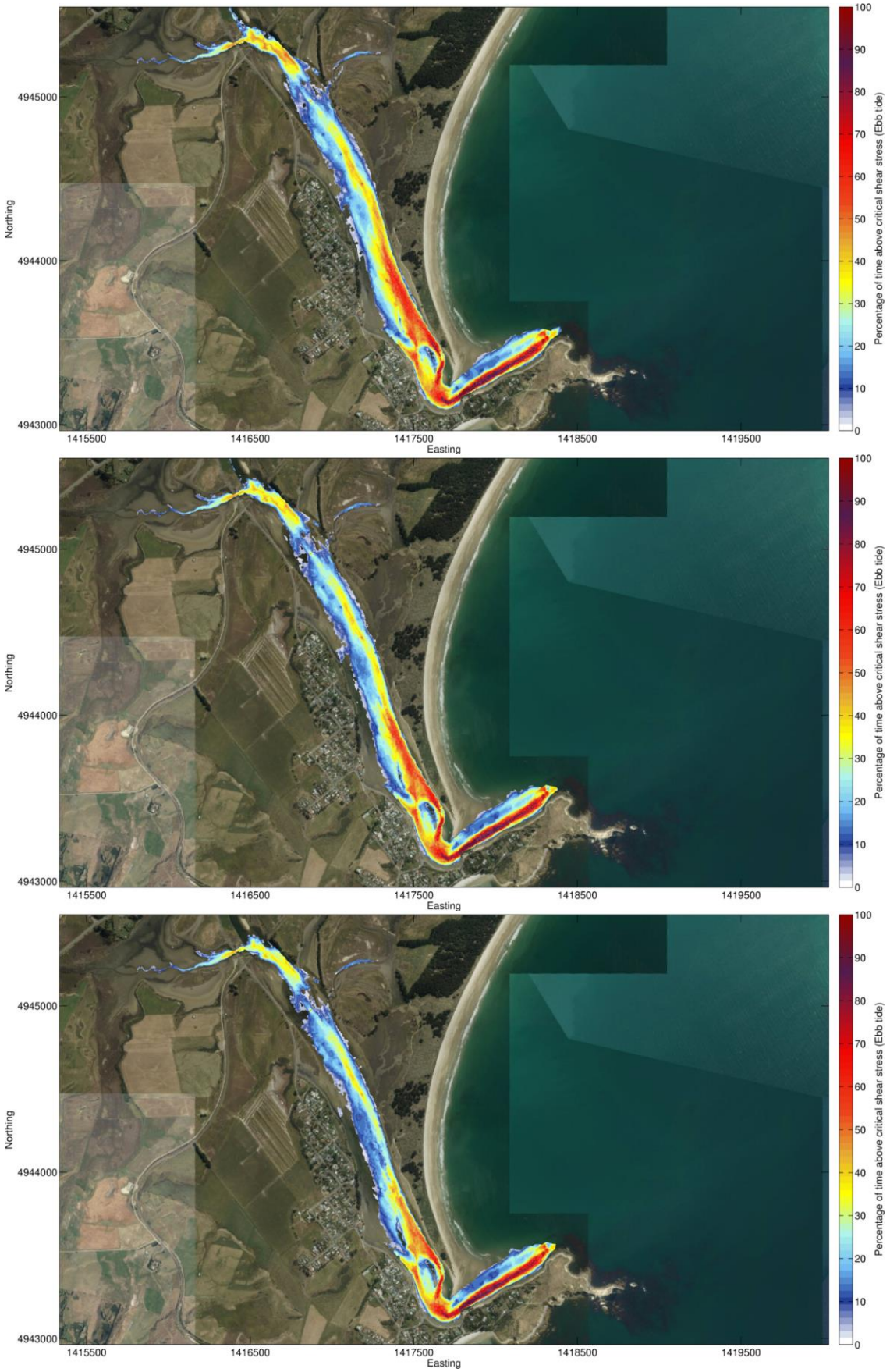

Figure 4.6 Percentage of time the critical bed shear stress is exceeded in spring tide during ebb flow for D50 grain size value of 50 (top), 100 (middle) and 200 (bottom) microns.

4.2. Tidal volumes

A hypsographic curve (Figure 4.7) has been produced for the estuary, based on a one-month simulation that included the measured river flows. This curve makes an estimate of the total volume of water in the estuary at different stages of tide. The maximum spring tidal volume is approximately 1.1 M m^3 while the neap volume is around 0.85 M m^3.

Multiple cross sectional data of the upper, mid and lower parts of the estuary are provided for representative stages of the tide in Figure 4.8. An inundation map of the estuary is presented in Figure 4.9, showing the number of hours the seabed is wetted over the tidal cycle.

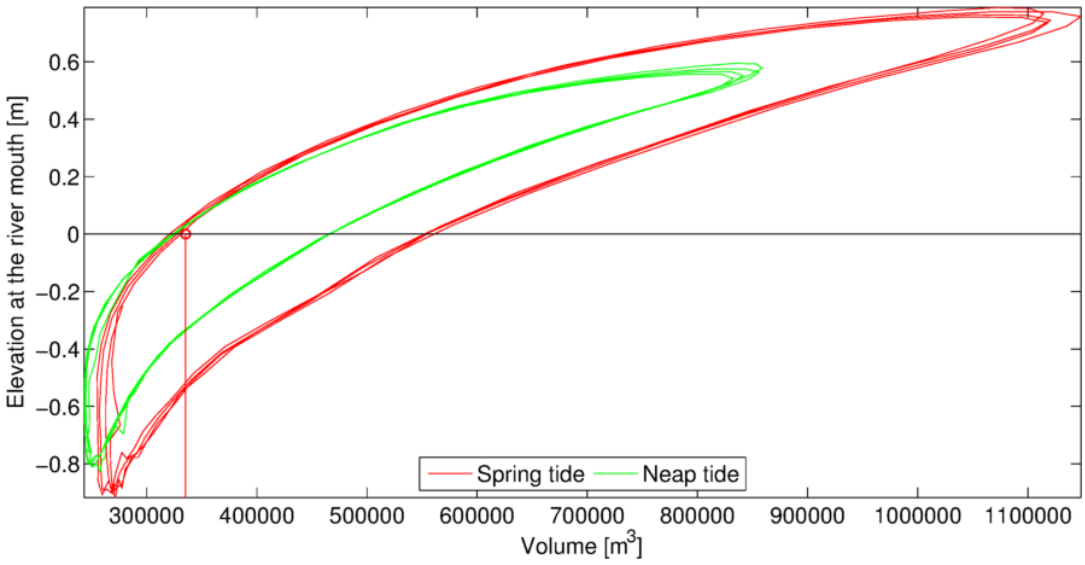

Figure 4.7 Hypsographic curve defined from a one-month simulation. Using this curve, the volume of water in the estuary can be estimated for a given tide level on a rising or falling tide, at spring or neap.

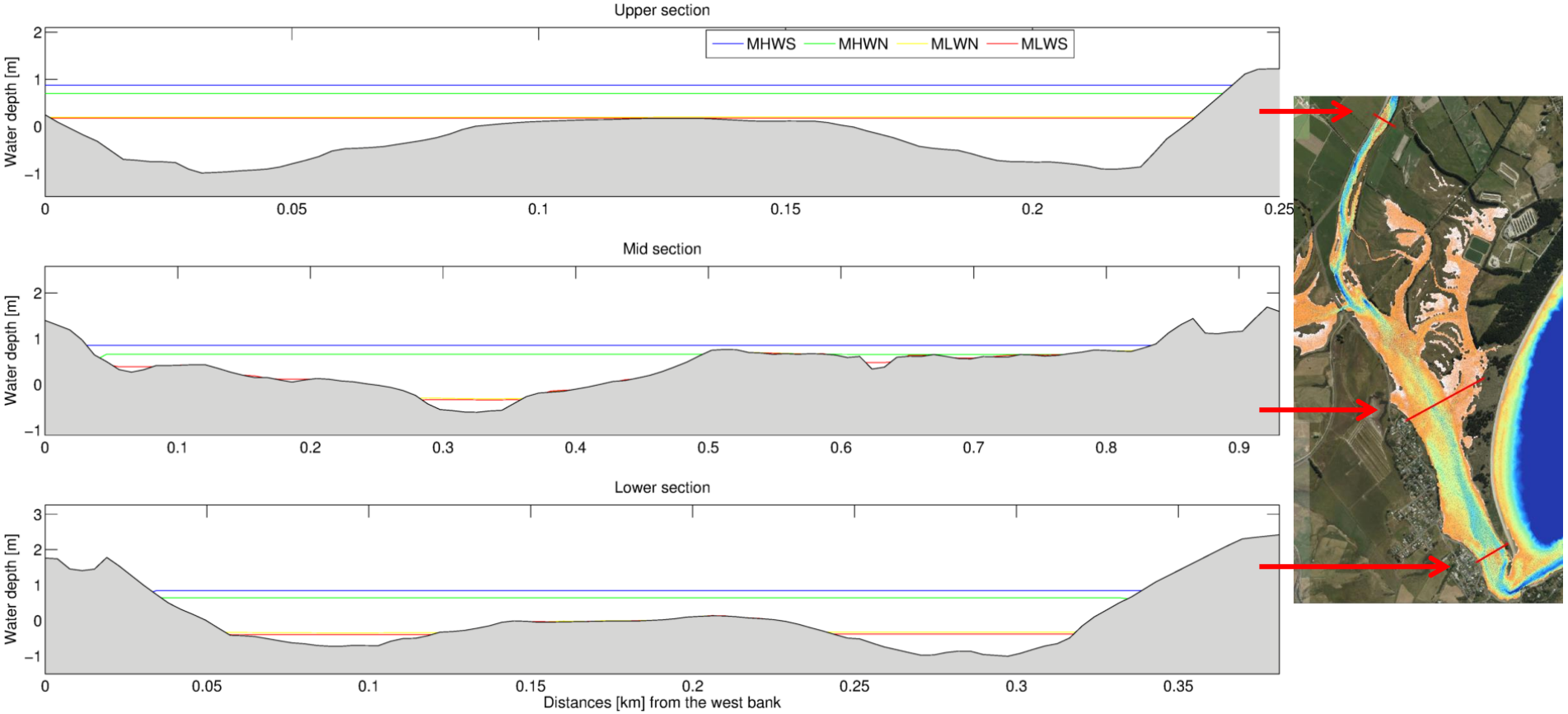

Figure 4.8 Cross sectional profiles of the upper, mid and lower estuary, with tide levels noted.

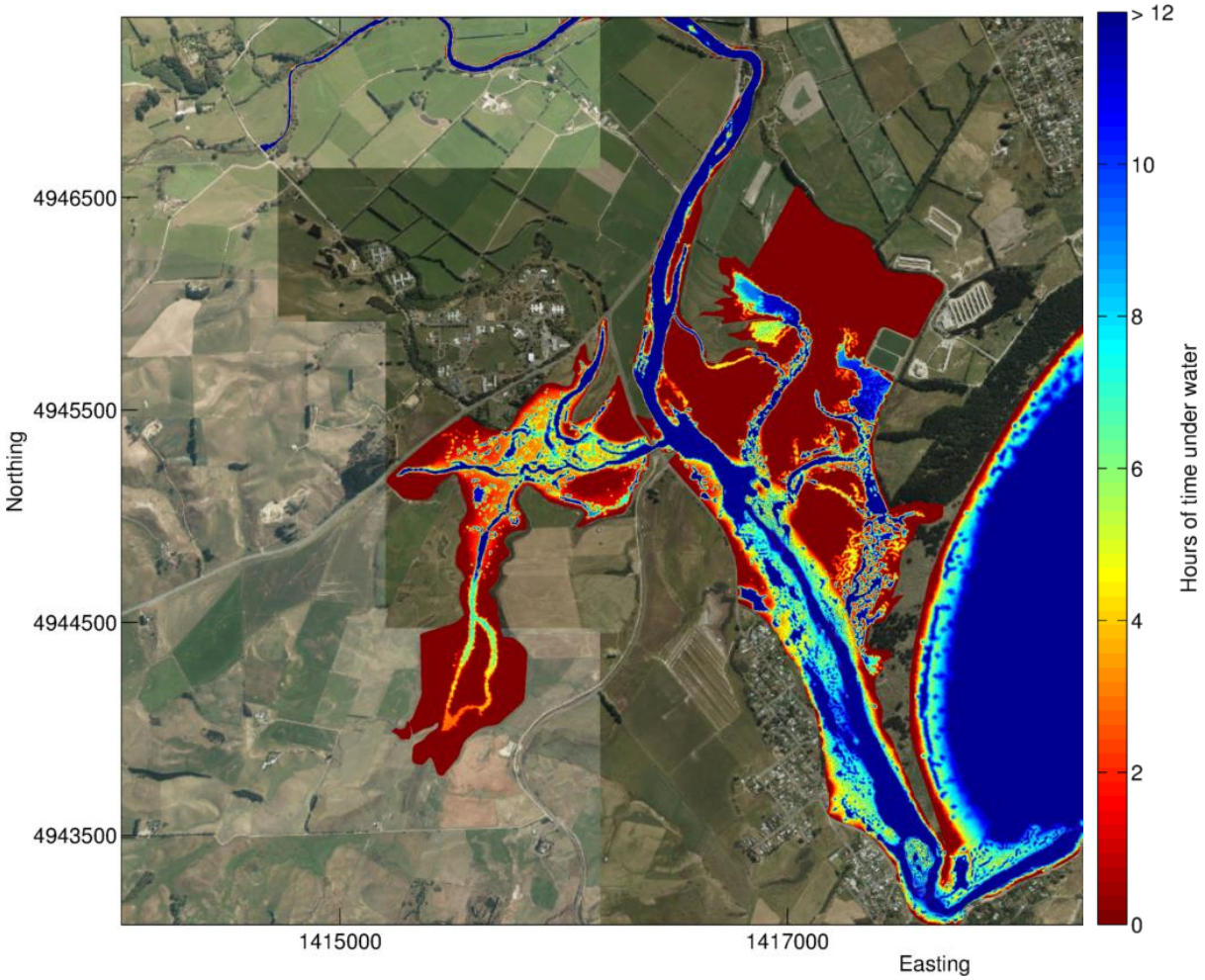

Figure 4.9 Inundation map of the estuary, showing the number of hours wetted per spring tidal cycle.

4.3. Water properties

4.3.1. Salinity

An assessment of the influence of seawater on dilution in the estuary has been made by considering the depth-averaged salinity at high and low tides for the spring and neap tidal states at the three low flow rates (i.e. 129, 220 and 350 l/s). These are shown on Figure 4.10 to Figure 4.12, while the salinity difference between the water surface and seabed level are shown on Figure 4.13 and Figure 4.14 both for spring and neap tides, at high and low tide respectively.

These data show that the primary mixing zone between the salty and fresh waters varies between spring and neap tides. On a spring tide, the model indicates the salt wedge penetrates almost as far as Orbell's Crossing, which is broadly consistent with the salinity measurements made in the upper estuary. Increasing the river flow in the model from 129 l/s to 350 l/s moves the penetration of the salty wedge downstream by some 500-600 m (see Figure 4.11). At low tide there is still salty water present between Orbell and State Highway (Figure 4.12) and the salt water penetration increases by around 500 m over the three river flow scenarios, with greater penetration during the lower flows. The model predicts saline stratification within the mixing zone (Figure 4.13 and Figure 4.14) which is broadly consistent with the observations (see Figure 2.5).

The river flows tested here have very little effect on the salinity spatial distributions in the lower estuary (i.e. downstream of the Railway bridge) or on the governing hydrodynamics. On that basis the 350 l/s low river flow scenario was applied in the following model simulations for the estuarine water properties.

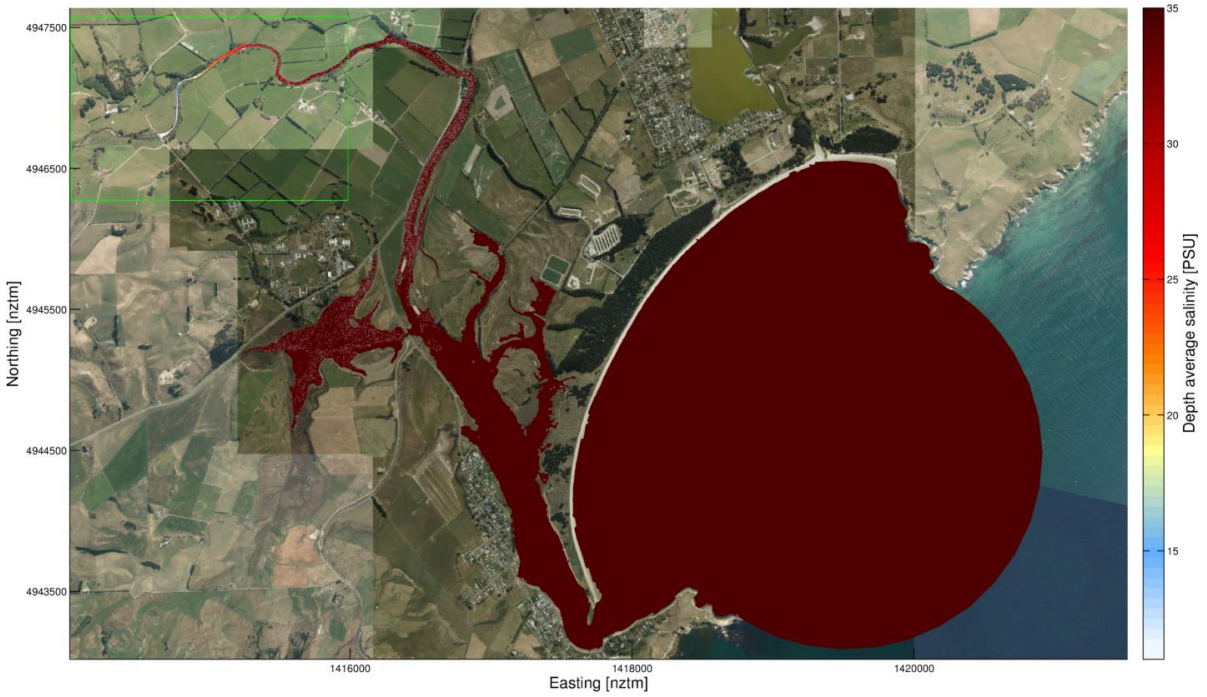

Figure 4.10 Depth-averaged salinity at high tide during a spring tide with river flow of 350 l/s. Note that the mixing zone is concentrated downstream of Orbell's Crossing.

Figure 4.11 Depth-averaged salinity at high tide near Orbell's Crossing for spring (top) and neap (bottom) tide at 129 (left), 220 (middle) and 350 (right) l/s.

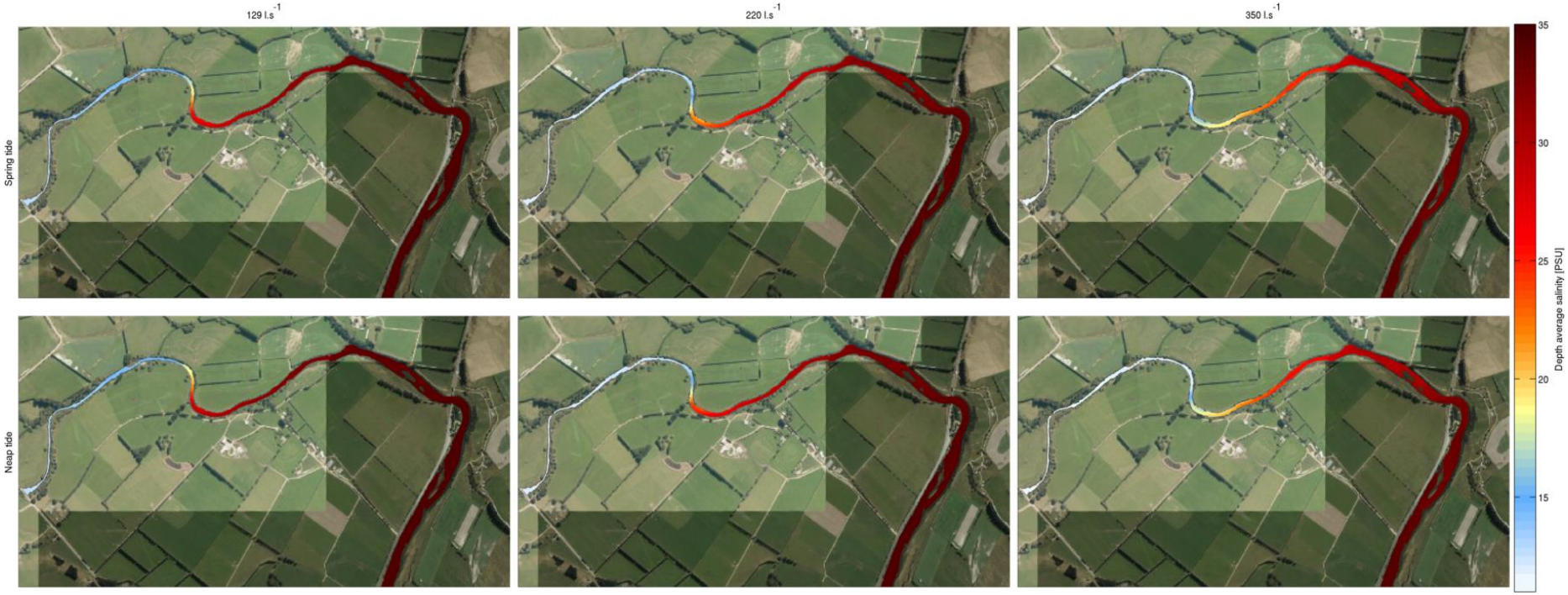

Figure 4.12 Depth-averaged salinity at low tide between Orbell's Crossing and State Highway site for spring (top) and neap (bottom) tide at 129 (left), 220 (middle) and 350 (right) l/s.

Figure 4.13 Salinity difference (in PSU) between surface layer and the bottom layer at high tide near Orbell's Crossing for spring tide (top) and neap tide (bottom) at 129 (left), 220 (middle) and 350 (right) l/s.

Figure 4.14 Salinity difference (in PSU) between surface layer and the bottom layer at low tide near Orbell's Crossing for spring tide (top) and neap tide (bottom) at 129 (left), 220 (middle) and 350 (right) l/s.

4.3.1. River water dilution and estuarine residence time

Water age (or residence time) and nutrient concentration levels from the river input to the estuary have been defined with the model using Eulerian tracers (see Section 3.3).

The relative (or normalised) concentration of river nutrient after 24 and 48 hours of continuous release under the three river flow states during spring tide are presented in Figure 4.15 and Figure 4.17, while the same data is represented in terms of the dilution in Figure 4.16 and Figure 4.18. A normalised concentration is one where the highest concentration, i.e. at the source (Orbell's Crossing), is set to 1.

The results show that while the differences between the three flow rates are quite small, the effect of increasing the river flow from 129 to 350 l/s is still apparent in the concentration and dilution outcomes. Note that because the volume of river water supplied to the estuary is very small compared with the tidal fluxes, the effect of increasing the river flows does not affect the estuarine hydrodynamics but it does increase the input of tracer (e.g. nutrients). What are being demonstrated on Figures 4.15 to 4.18 are the dilution characteristics of the estuary as the input volume increases. Ultimately however, for the summer low flow rates tested here the tidal exchange dominates the mixing dynamics in the middle and lower regions of the estuary.

A further examination of the dilution characteristics of the estuary is presented on Figure 4.19 and Figure 4.20. Here, the predicted dilution following a discrete pollution event from the river is shown at the surface and bottom of the water column after 2, 6 and 10 tidal cycles for spring and neap tides, respectively. After 2 tidal cycles, the estuary between the State Highway and the Railway bridges still has very low dilution (less than 10%) for the entire water column, while the lower estuary has around 50% dilution along the main channel. After 10 tidal cycles, just upstream of the Railway bridge the dilution only reaches 60% while in the lower estuary it approaches 100%. While the spring tide range presents slightly higher dilution rates than the neap tide, the vicinity of the State Highway bridge has the lowest capacity for flushing under this particular pollution scenario.

The water age, in days, under spring and neap tide conditions are presented in Figure 4.21 and Figure 4.22, respectively. Note that both the sea and the river are considered to be sources in this type of tracer simulation. Water age is computed as a time-average for each part of the model, so understandably the intertidal areas tend to have lower values because water cannot be resident during large parts of the tidal cycle. There are also some areas where water is trapped in pools despite only being wet for very short periods over the tide. Nonetheless, despite the limitations of this technique it is useful way to examine the typical residence times for the water sources.

In the upper estuary, water age increases proportional to the distance from the freshwater tracer source. In the mid region, where both fresh and the seawater are tracer sources, the spring tide age was only slightly higher (7-8 days) than the lower estuary (6-7 days). During neap tide, the water age in the mid and lower estuary is around 2 days older than for spring, reflecting the increased exchange in the estuary due to the larger tides.

Figure 4.15 Relative (normalised) concentration of river nutrient after 24H of continuous release from Orbell's Crossing under the three flow states during spring tide. The release was started at the peak ebb tide.

Figure 4.16 Dilution of river nutrient after 24H of continuous release Orbell's Crossing under the three flow states during spring tide. The release was started at the peak ebb tide..

Figure 4.17 Relative (normalised) concentration of river nutrient after 48H of continuous release Orbell's Crossing under the three flow states during spring tide. The release was started at the peak ebb tide.

Figure 4.18 Dilution of river nutrient after 48H of continuous release Orbell's Crossing under the three flow states during spring tide. The release was started at the peak ebb tide.

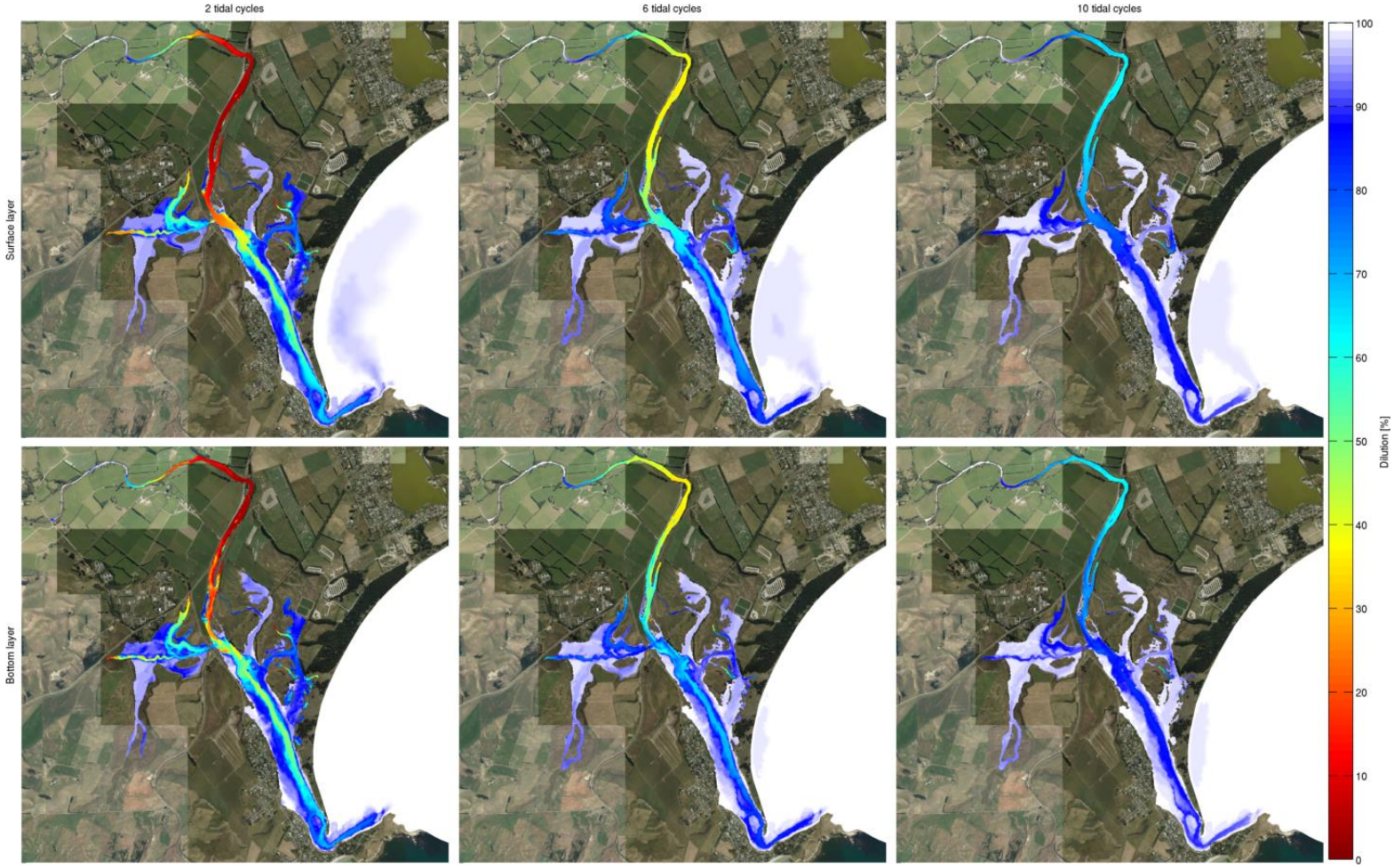

Figure 4.19 Dilution occurring at the surface (top) and bottom (bottom) of the estuary after 2 (left), 6 (middle) and 10 tidal cycles during a spring tide range. The scenario modelled here is a discrete release of pollutant from the river into the estuary.

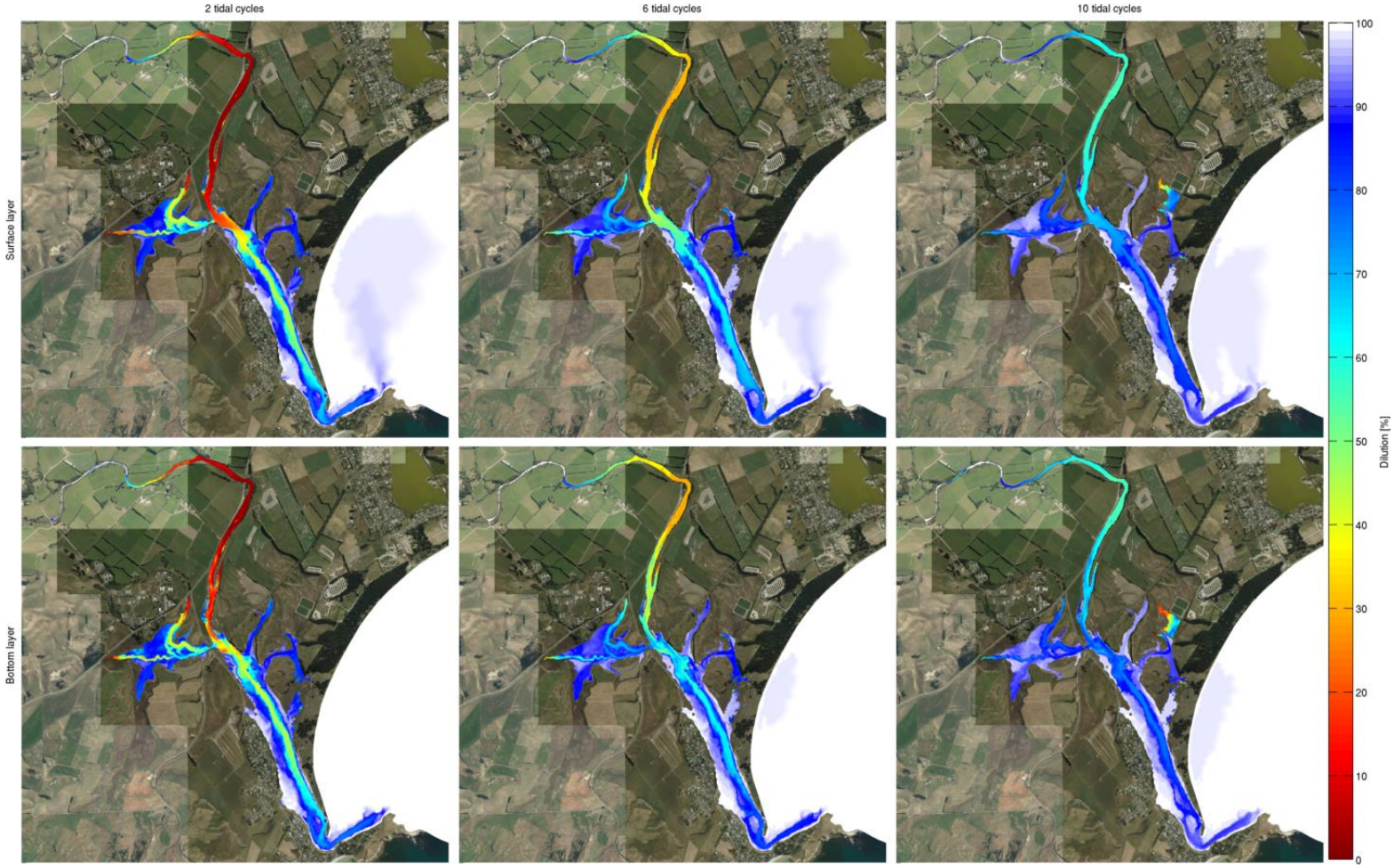

Figure 4.20 Dilution occurring at the surface (top) and bottom (bottom) of the estuary after 2 (left), 6 (middle) and 10 tidal cycles during a neap tide range. The scenario modelled here is a discrete release of pollutant from the river into the estuary.

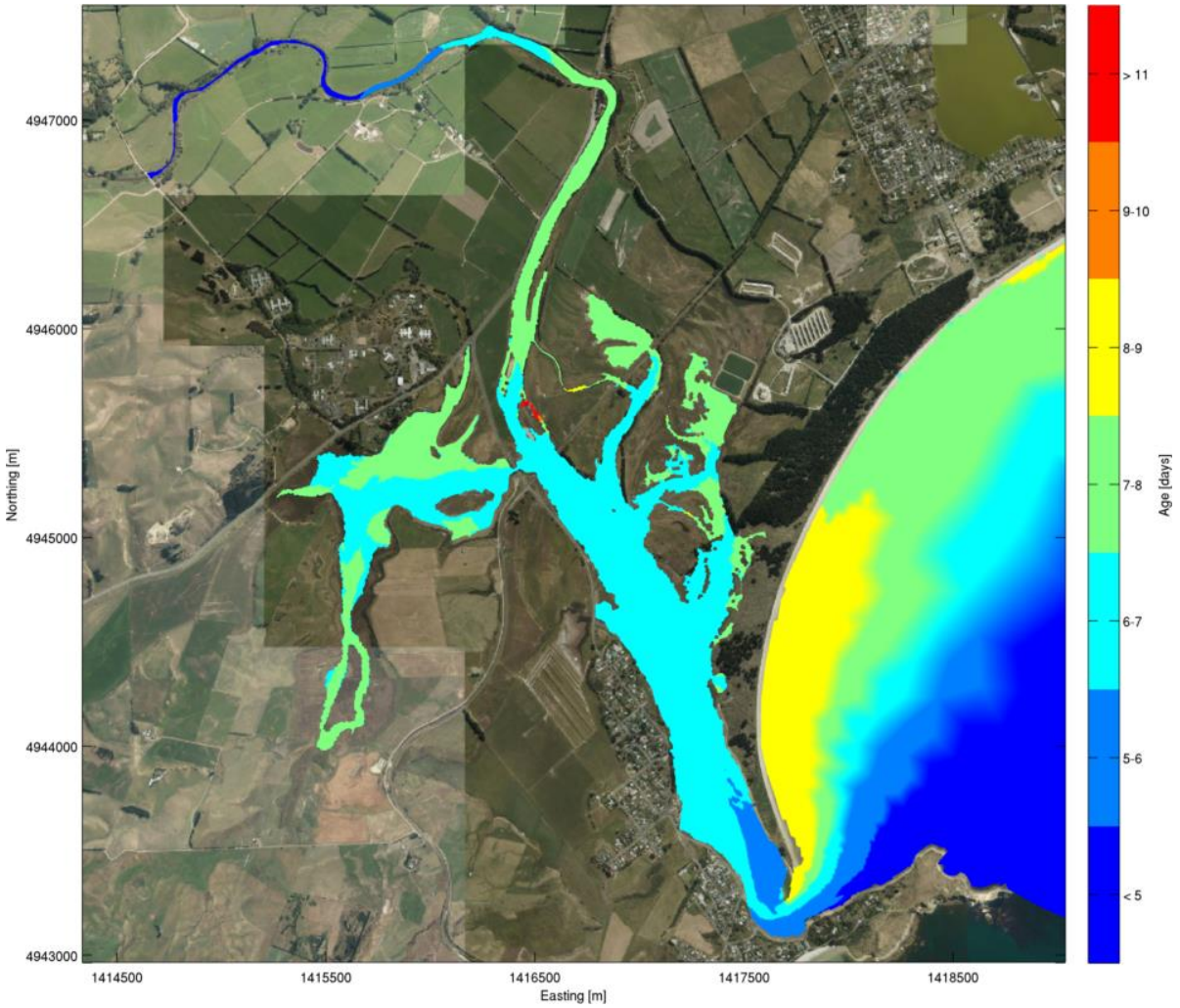

Figure 4.21 Water age (in days) under spring tide conditions. Note that both the sea and the river are considered to be sources of water to the estuary in this analysis.

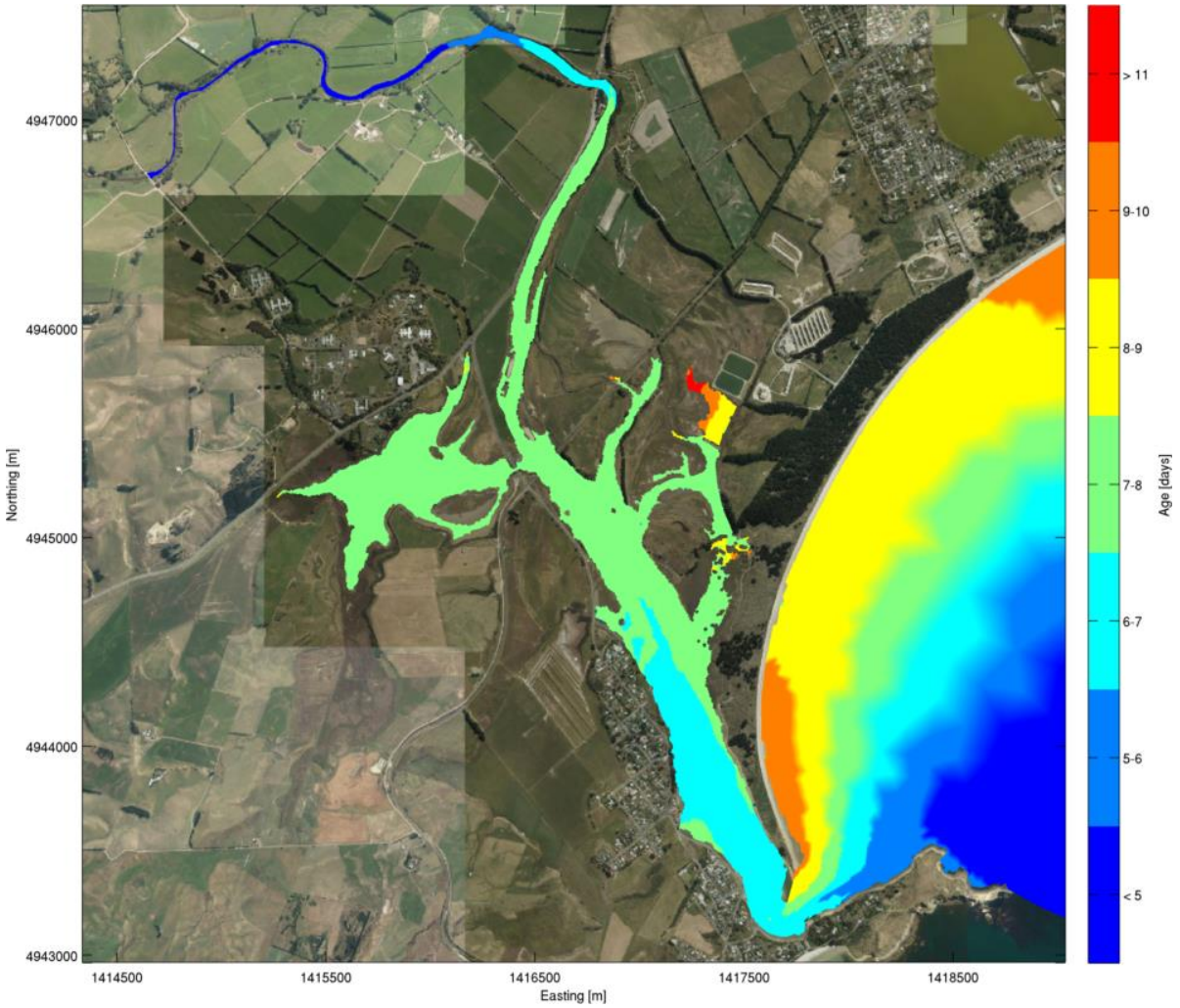

Figure 4.22 Water age (in days) under neap tide conditions. Note that both the sea and the river are considered to be sources of water to the estuary in this analysis.

5. SUMMARY

An assessment of the influence of the typical summer low river flows on the physical and chemical conditions of the Waikouaiti estuary has been made, fulfilling stages 1 and 2 of an initial study programme. A hydrographic survey of the estuary was undertaken and those data were combined with other bathymetric and topographic measurements to form the basis of a numerical model of the estuary. Observations were obtained to provide appropriate data for hydrodynamic model validation and the boundary conditions for implementation. The sensitivity tests provided satisfactory validation against observed water levels and current speeds at several locations within the estuary.

The model is based on open source code which is freely available. All the measured data, model setup, boundary conditions and configuration files are also available for community use. While this report documents the initial model establishment, it is expected that improvements to the model will be made over time as other users become involved in the model development and more data becomes available for validation. The ultimate goal is for the model to become a useful tool for the community to further understand how the estuarine hydrodynamics affect the ecosystem processes.

Governing dynamics

The model results provide an initial characterisation of the primary hydrodynamic processes in the estuary. The tidal flow regime was modelled under spring and neap tide scenarios with river flow rates of 129, 220 and 350 l/s. In terms of the overall hydrodynamics, the effect of river flows up to 350 l/s was found to be negligible, and the tidal component dominated the estuary hydrodynamics over the low flow summer scenarios examined. Accordingly, the higher river flow regime of 350 l/s was used to assess the spring and neap tide current flow patterns as well as the potential for sediment mobility and the sediment transport capacity within the estuary. Currents impart a stress on the estuary sediments, and when that stress exceeds an entrainment threshold, the sediments can be mobilised and transported by the flows. A series of maps have been produced to show currents, sediment mobility and transport capacity; clearly illustrating the asymmetry between the ebb and flood tidal stages, and the difference in magnitude over the neap and spring tidal range.

The net consequence of the strong tidal asymmetry in mobilising and entraining the bed sediments leads to a sorting of the grain sizes over time. Coarse material requires higher current flows to mobilise than fine material, and the duration of the flow above the critical entrainment level is important to the sediment transport outcomes for each grain size fraction. The patterns of potential sediment mobility for silt and fine sand has been characterised within the estuary, showing that even the smaller channels have flows that can entrain silts and sands for considerable periods of time on each tide. However the adjacent shallow intertidal flats do not and these areas are accordingly more susceptible to siltation.

Tidal volumes have been calculated for the whole estuary, along with an inundation map to show the number of hours the seabed is wetted over each tidal cycle.

Salinity

An assessment of the influence of seawater on dilution in the estuary has been made by considering the depth-averaged salinity at high and low tides for the spring and neap tidal states at the three low river flow rates. The results show that the position of the primary mixing zone between the salty and fresh waters varies around 500-600 m over the spring / neap range. On a spring tide at 129 l/s river flow, the salt wedge penetrates almost as far upstream as Orbell's Crossing, and increasing the river flow from 129 l/s to 350 l/s reduces the upstream penetration of the salty wedge by some 500 m. At low tide under the river flows tested here, salty water is still present between Orbell's Crossing and the State Highway bridge. The summer low flow rates have little effect on the depth-average salinity in middle and lower parts of the estuary (i.e. below State Highway bridge). However, considering the stratified water column, the effect of the higher flows is evident further downstream, but not beyond the Railway bridge. In other words, the summer low flows maintain a salty estuary downstream of the Railway bridge. For the zone between the two bridges, at low tide there can be a less saline surface layer present and the downstream extent of that layer varies according to the river flow rate (i.e. 129-350 l/s).

River water dilution and estuarine residence times

The behaviour of freshwater along the estuary was estimated by calculating the dilution and water age using a tracer method. Dilution maps were produced after 2, 6 and 10 full tidal cycles, showing how the river water becomes diluted over time in different parts of the estuary. Water age indicates the time elapsed since the tracer left the source, and here the open ocean and the river were both considered to be water sources to the estuary.

The results show that while increasing the river flow from 129 to 350 l/s has an observable effect on the dilution outcomes, this is only because the total input of tracer (e.g. nutrient) from the river increases proportionally. If the same amount of tracer (or nutrient) was supplied but diluted by the higher river flows, then the effect of increased river flow would be negligible. Notably, the volume of river water supplied to the estuary in these summer low flows remains very small compared with the volume from the tidal fluxes, and therefore increasing the river flows does not materially affect the wider estuarine hydrodynamics.

Considering a discrete pollution event sourced from the river, after 2 tidal cycles, the estuary between the State Highway and the Railway bridges still has very low dilution (less than 10%) for the entire water column, while the lower estuary below the Railway bridge has around 50% dilution along the main channel. After 10 tidal cycles, just upstream of the Railway bridge the dilution still only reaches around 60% while in the lower estuary it approaches 100%. While the spring tide range presents slightly higher dilution rates than the neap tide, the vicinity of the State Highway bridge has the lowest capacity for flushing under this particular pollution scenario.

Upstream of the State Highway bridge, water age increases proportional to the distance from the freshwater source at Orbell's Crossing. In the mid region between the two bridges where both fresh and the seawater are sources, the spring tide age was only slightly higher (7-8 days) than the lower estuary (6-7 days). During neap tide, the water age in the mid and lower estuary is around 2 days older than for spring, reflecting the increased exchange in the estuary due to the larger tides.

REFERENCES

Andrejev, O., Myrberg, K., Lundberg, P.A., 2004. Age and renewal time of water masses in a semi-enclosed basin – application to the Gulf of Finland. Tellus 56, 548–558.

Deleersnijder, E., Campin, J.-M., Delhez, E.J.M., 2001. The concept of age in marine modelling. I. Theory and preliminary model results. J. Mar. Syst. 25, 229–267. doi:10.1016/S0924-7963(01)00026-4

Hall, T.M., Haine, T.W.N., 2002. On Ocean Transport Diagnostics: The Idealized Age Tracer and the Age Spectrum. J. Phys. Oceanogr. 32, 1987–1991. doi:http://dx.doi.org/10.1175/1520-0485(2002)032<1987:OOTDTI>2.0.CO;2

Meier, H.E.M., Höglund, A., 2013. Studying the Baltic Sea Circulation with Eulerian Tracers, in: Preventive Methods for Coastal Protection. Springer International Publishing, pp. 101–129.

Zhang, W.G., Wilkin, J.L., Schofield, O.M.E., 2010. Simulation of water age and residence time in New York Bight. J. Phys. Oceanogr. 40, 965–982. doi:http://dx.doi.org/10.1175/2009JPO4249.1

Zhang, Y.L., Baptista, A.M., 2008. A semi-implicit Eulerian-Lagrangian finite element model for cross-scale ocean circulation. Ocean Model. 21, 71–96.

APPENDIX ONE – SURVEY REPORT

Waikouaiti Estuary - March 2016

BRIEF

Acting on instruction of Brett Beamsley of MetOacean, HHS carried out survey of the following areas:

Entrance Channel at Karitane

Waikouaiti river from Karitane Entrance to Orbell Crossing at McGrath Road.

Waikouaiti river and swamp area between SH1, Coast Road and Merton Station Road.

Survey transects were as per email Brett Beamsley.

EQUIPMENT USED

The Equipment used included Trimble R8 and 5700 RTK receivers, Trimble R8 RTK base station, Reson 210 and Reson 415 echo sounders, Trimble HydroPro software, survey vessel “Seaquill”, Smartwave dinghy and Terramodel and HydroPRO being used for data reduction.

PERSONNEL

The personnel involved included myself (P G Hunter) with A N Sutherland and R K Brooks.

SQUAT / SWELL / TIDE

RTK reduced level survey methodology was used to gather spot heights, both on water and land. This technique eliminates the need determine water level data and subsequently allow for variations such as squat, swell and tide in reduction.

BAR CHECK

Due to the shallow nature of the site and the changing salinity/temp of the water column the echo sounder calibration was limited to draft and SV constants being used. The system output was checked against spot observations

POSITION CHECK

RTK total station calibration was confirmed by visiting two high vertical order bench marks on SH1. Perhaps surprisingly, as these trigs had low horizontal precision, the horizontal check was also very good.

VERTICAL DATUM

All surveys were reduced to MSL. System was set using Trig A26F which had a 4^{th} order vertical height of 41.79m

GEODESY

Data is provided reduced to North Taieri GD2000.

NZVD2009 was used in calculation of ellipsoid geoid residuals and applied to levels post survey.

SITE CONDITIONS

The sites were worked with respect to prevailing conditions. Survey was carried during the period out of 08-13/03/2016 when wind and water levels permitted, and only during daylight hours. Flotsam was an issue as were impassable bog areas, overhanging trees, steep banks and electric fences. In the entrance channel swell and standing waves were a hindrance.

QA/QC

A check of the correlation between all cross lines was excellent. Cross checks with differing systems were excellent as were checks at other BM's.

DELIVERIABLES

All surveyed areas have been supplied in either DXF or DWG format.

SURVEY STATEMENT/DECLARATION

The surveys were carried out with results to my satisfaction. Confidence levels for this work are better than 0.1m horizontal and 0.1m vertical.

Peter Gavin Hunter

Manager

HUNTER HYDROGRAPHIC SERVICES

Dated: (18/03/2016)